C. R. Mecanique 346 (2018) 678–700

Contents lists available at ScienceDirect

Comptes Rendus Mecanique

www.sciencedirect.com

Computational modeling of material forming processes / Simulation numérique des procédés de mise en forme

Effect of the kinematic hardening on the plastic anisotropy parameters for metallic sheets

Houssem Badreddine [a,*], Khemais Saanouni [a], Carl Labergère [a], Jean-Louis Duval [b]

[a] ICD/LASMIS, UMR 6281, University of Technology of Troyes, 12, rue Marie-Curie, CS 42060, 10004 Troyes cedex, France
[b] ESI Group Rungis, Parc d'affaires SILIC, 99, rue des Solets, BP 80112, 94513 Rungis cedex, France

ARTICLE INFO

Article history:
Received 18 October 2017
Accepted 9 April 2018
Available online 30 June 2018

Keywords:
Initial plastic anisotropy
Non-linear kinematic hardening
Finite strains
Strain and stress ratios

ABSTRACT

The initial plastic anisotropy parameters are conventionally determined from the Lankford strain ratios defined by $r^{\psi} = \frac{\varepsilon_{22}^{p\psi}}{\varepsilon_{33}^{p\psi}}$ (ψ being the direction of the loading path). They are usually considered as constant parameters that are determined at a given value of the plastic strain far from the early stage of the plastic flow (i.e. equivalent plastic strain of $\varepsilon_{eq}^{p} = 0.2\%$) and typically at an equivalent plastic strain in between 20% and 50% of plastic strain failure (or material ductility). What prompts to question about the relevance of this determination, considering that this ratio does not remain constant, but changes with plastic strain. Accordingly, when the nonlinear evolution of the kinematic hardening is accounted for, the Lankford strain ratios are expected to evolve significantly during the plastic flow.

In this work, a parametric study is performed to investigate the effect of the nonlinear kinematic hardening evolution of the Lankford strain ratios for different values of the kinematic hardening parameters. For the sake of clarity, this nonlinear kinematic hardening is formulated together with nonlinear isotropic hardening in the framework of anisotropic Hill-type (1948) yield criterion. Extension to other quadratic or non-quadratic yield criteria can be made without any difficulty. This parametric study is completed by studying the effect of these parameters on simulations of sheet metal forming by large plastic strains.

Notation

- RFF: Rotating frame formulation,
- TIP: Thermodynamics of the irreversible processes
- First-rank tensor or vector: $\vec{x}$, x_i,
- Second-rank tensor: $\underline{x}$, x_{ij},
- Fourth-rank tensor: $\underline{\underline{x}}$, x_{ijkl},
- Second-rank identity tensor: $\underline{1}$, δ_{ij},
- Fourth-rank symmetric identity tensor: $\underline{\underline{I}}$, $I_{ijkl} = \frac{1}{2}(\delta_{ik}\delta_{jl} + \delta_{il}\delta_{jk})$,

* Corresponding author.
E-mail address: houssem.badreddine@utt.fr (H. Badreddine).

https://doi.org/10.1016/j.crme.2018.06.004

- Fourth-rank symmetric deviatoric identity tensor: $\underline{\underline{I}}^{\mathrm{D}}$, $I^{\mathrm{D}}_{ijkl} = \frac{1}{2}(\delta_{ik}\delta_{jl} + \delta_{il}\delta_{jk}) - \frac{1}{3}\delta_{ij}\delta_{kl}$,
- Transpose of second-rank tensor: $\underline{x}^{\mathsf{T}}$, $(x_{ij})^{\mathsf{T}} = x_{ji}$,
- Symmetric and skew-symmetric parts of second-rank tensor: $\underline{x} = [\underline{x}]^{\mathrm{S}} + [\underline{x}]^{\mathrm{A}}$

$$[\underline{x}]^{\mathrm{S}} = \frac{1}{2}\left(\underline{x} + \underline{x}^{\mathsf{T}}\right),\ [\underline{x}]^{\mathrm{A}} = \frac{1}{2}\left(\underline{x} - \underline{x}^{\mathsf{T}}\right),$$

- Hydrostatic part of second-rank tensor: $[\underline{x}]^{\mathrm{H}} = \frac{1}{3}tr(\underline{x})\underline{1}$,
- Deviatoric part of second-rank tensor: $[\underline{x}]^{\mathrm{D}} = \underline{x} - [\underline{x}]^{\mathrm{H}}$,
- Inverse of second-rank tensor: $\underline{x}^{-1}, x^{-1}_{ij}$,
- Inverse of fourth-rank tensor: $\underline{\underline{x}}^{-1}$, x^{-1}_{ijkl},
- Time derivative of second-rank tensor: $\dot{\underline{x}}$, $\dot{x}_{ij}$,
- Simple contraction of two second-rank tensors: $z_{ij} = x_{ik}y_{kj}$,
- Double contraction of two second-rank tensors: $z = \underline{x} : \underline{y} = x_{ij}y_{ji}$,
- Tensorial product of two second-rank tensors: $\underline{\underline{z}} = \underline{x} \otimes \underline{y}$, $z_{ijkl} = x_{ij}y_{kl}$,
- The trace of the second-rank tensor (1st invariant): $x_I = tr(\underline{x}) = x_{kk}$,
- Second invariant of the second-rank tensor: $x_{II} = [tr^2(\underline{x}) - tr(\underline{x}^2)]/2$,
- Determinant of the second-rank tensor (3rd invariant): $det(\underline{x})$,
- Rotated second-rank tensor (with rigid body rotation $\underline{Q}$): $\bar{\underline{x}} = \underline{Q}^{\mathsf{T}}.\underline{x}.\underline{Q}$, $\bar{x}_{ij} = Q_{ki}Q_{lj}\underline{x}_{kl}$,
- Rotated fourth-rank tensor between isocline and current configurations: $\bar{\underline{\underline{x}}} = (\underline{Q}^{\mathsf{T}} \otimes \underline{Q}) : \underline{x} : (\underline{Q} \otimes \underline{Q}^{\mathsf{T}})$, or $\bar{x}_{ijkl} = Q_{ri}Q_{sj}Q_{pk}Q_{ql}x_{ijkl}$.

1. Introduction

Lightweight structural components, needed for many industrial sectors as automotive and aerospace industries, require advanced High Strength Materials (AHSM) such as steels and aluminum alloys. However, because of their low ductility at room temperature, the forming of such types of materials by deep drawing presents several difficulties. Among these difficulties, we find springback, which appears at the end of the deep drawing operation, when the stamping tools are removed. Considerable efforts have been made to predict numerically, with the best accuracy, the springback in sheet metal forming. For a better numerical prediction of the springback, several factors have been studied. Among them, the most important one is the development of constitutive equations to predict the plastic flow under various loading paths as can be found in [1–11]. The mechanical responses of the high-strength materials under complex loading paths as reverse loading–unloading–reloading must be considered for accurate springback simulations involving accurate modeling of the plastic flow and the related various types of work hardening as well as initial and induced anisotropies. In fact, the metal sheets subjected to deep drawing locally exhibit complex loading paths due mainly to bending–unbending. Therefore, the behavior of the material under loading–unloading–reverse loading must be accurately predicted, in addition to the material behavior under usual monotonic simple (1D) loading paths. Because these strain properties cannot be captured by traditional isotropic hardening models, the current tendency is to consider kinematic hardening models. A better description of the stress–strain responses under reverse loading was then proposed by Armstrong and Frederick [12], introducing a non-linear description of the kinematic hardening with the addition of a dynamic recovery terms. This model has been improved further by Chaboche [13] to describe the ratcheting effects during cyclic loading. Teodosiu et al. [14,15] used a kinematic hardening based on a tensor description of dislocation structures growing under the change of loading paths or change of strain path to better reflect the microscopic changes that occur during plastic flow.

Various kinematic hardening models have been implemented to be used in the FEM simulations of sheet metal forming in order to predict as accurately as possible the formability and springback phenomena [3,4,7–11,16–22]. Other approaches have been developed based on classical nonlinear kinematic hardening combined with the distortion of the subsequent yield surfaces [23–30]. More recently, without using the concept of kinematic hardening, a uniform yield surface based on an anisotropic hardening (HAH) was proposed by Barlat et al. [1,2].

Moreover, considering kinematic hardening in the context of anisotropic plastic flow brings out the issue of identification of the anisotropy parameters. Indeed, the latter are conventionally determined using either the Lankford (strain) and/or stress ratios [17,20,31–41]. When making this identification, it is usual to assume that these coefficients are constant during plastic flow. This assumption is valid for models taking into account isotropic hardening. However, when accounting for kinematic hardening, this assumption is no longer valid, as it has been shown in the work by Wu et al. [21].

In this paper, the sensitivity of Lankford strain ratios evolution according to kinematic hardening parameters and its impact on the simulation of thin sheets forming processes is parametrically studied. In the second section, the theoretical framework for the formulation, under large plastic strains, of the anisotropic elastic–plastic constitutive equations accounting for nonlinear mixed (isotropic and kinematic) hardening is presented. In this context, the anisotropy of the plastic flow and that of the yield function are unified by the same anisotropy parameters. In the third section an exhaustive sensitivity analysis of the evolution of Lankford ratios with respect to the kinematic hardening parameters is performed through a parametric study.

Table 1
State and associated variables.

Phenomena	State variables	Associated variables
Elastoplasticity	ε^{e}_{ij} or ε^{p}_{ij}	σ_{ij}
Kinematic hardening	α_{ij}	X_{ij}
Isotropic hardening	r	R

2. Presentation of the plastic anisotropic constitutive equations with kinematic hardening

This model is defined in the framework of large plastic strain assumption for which elastoplastic kinematics is defined using the classical multiplicative decomposition of the total gradient F_{ij} into elastic F^{e}_{ij} and plastic F^{p}_{ij} parts, i.e. $F_{ij} = F^{e}_{ik}F^{p}_{kj}$ [42–47]. To satisfy the objectivity requirement including plastic anisotropy, the RFF (Rotated Frame Formulation) is used, for which all the mechanical variables and their evolution equations are formulated on an intermediate locally rotated "isocline" configuration. This specific configuration conserves the initial orientation of material directions, which are defined by the rigid body rotation tensor Q_{ij} with respect to the actual configuration [17,48,49], so that all the tensorial fields defined on the actual configuration (like tensors σ_{ij}, ε^{e}_{ij}, α_{ij}, $X_{ij}, \ldots$) are transported using the tensor Q_{ij} to and from the intermediate "isocline" configuration by $\bar{x}_{ij} = Q_{ki}x_{kl}Q_{lj}$. If the assumption of small elastic strains, which is verified for most metallic materials, is adopted, then this leads to the additive decomposition of the total strain rate tensor according to [17,48,49]:

$$D_{ij} = \varepsilon^{eJ}_{ij} + D^{p}_{ij} \tag{1}$$

In this work, the framework of thermodynamics of irreversible processes (TIP) is used to define the overall constitutive equations of anisotropic elastoplastic model under isothermal conditions. All phenomena considered are represented by a pair of state variables. As showed in Table 1, the following pairs of state variables are introduced: (i) $(\varepsilon^{e}_{ij}, \sigma_{ij})$ represents the elastoplastic flow; (ii) (α_{ij}, X_{ij}) represents the kinematic hardening depicting the translation of the yield surface center, and (iii) (r, R) represents the isotropic hardening depicting the change in the cross section of the yield surface.

In this framework of isothermal time-independent plasticity, the Helmholtz free energy $\Psi = \Psi(\varepsilon^{e}_{ij}, \alpha_{ij}, r)$, positive and convex function of all the strain-like state variables in the strain space, is taken as a state potential [48,50,51]. Assuming that the plastic strain and the hardening have no effect on the initial isotropic elastic properties of the material, the state potential can be additively decomposed as follows:

$$\rho\Psi = \rho\Psi^{e} + \rho\Psi^{p} = \frac{1}{2}\varepsilon^{e}_{mn}\Lambda_{mnpq}\varepsilon^{e}_{pq} + \frac{1}{3}C\alpha_{mn}\alpha_{mn} + \frac{1}{2}Qr^{2} \tag{2}$$

The stress-like variables are easily derived from the state potential according to:

$$\sigma_{ij} = \frac{\partial\rho\Psi}{\partial\varepsilon^{e}_{ij}} = 2\mu_{e}\varepsilon^{e}_{ij} + \lambda_{e}\varepsilon^{e}_{kk}\delta_{ij} \tag{3}$$

$$X_{ij} = \frac{\partial\rho\Psi}{\partial\alpha_{ij}} = \frac{2}{3}C\alpha_{ij} \tag{4}$$

$$R = \frac{\partial\rho\Psi}{\partial r} = Qr \tag{5}$$

Note that Eqs. (3)–(5) are extracted from the Clausius–Duhem inequality (combination of the first and second principles of thermodynamics) together with the residual dissipation inequality $\Phi = \sigma_{ij}D^{p}_{ij} - X_{ij}\dot{\alpha}_{ij} - R\dot{r} \geq 0$ to be fulfilled by all the constitutive equations (thermodynamic admissibility). In this inequality, the stress-like variables are given by the state relations (3)–(5), while their associated flux variables (D^{p}_{ij}, $\dot{\alpha}_{ij}$, and $\dot{r}$) have to be derived from a dissipation potential in such a manner that the above Clausius–Duhem inequality is identically satisfied. To achieve that, and in order to introduce nonlinear kinematic and isotropic hardenings in the framework of non-associative plasticity, a yield function $f(\sigma_{ij}, X_{ij}, R)$ and a plastic potential $F(\sigma_{ij}, X_{ij}, R)$ are introduced, both positive and convex functions of their main arguments in the stress space [48,52,53]. From these functions, the well-known evolution relationships are obtained by the generalized normality rule.

In this study, the quadratic Hill [38] yield function is used:

$$f(\sigma_{kl}, X_{kl}, R) = \|\sigma_{kl} - X_{kl}\|_{H} - R - \sigma_{y} = 0 \tag{6}$$

$$F(\sigma_{kl}, X_{kl}, R) = \|\sigma_{kl} - X_{kl}\|_{H} - R + \frac{3a}{4C}X_{kl}X_{kl} + \frac{b}{2Q}R^{2} \tag{7}$$

where $\|\underline{\sigma} - \underline{X}\|_{H} = \sqrt{(\sigma^{D}_{ij} - X_{ij})H_{ijkl}(\sigma^{D}_{ij} - X_{ij})}$ is the classical quadratic anisotropic Hill [38] equivalent stress characterized by a purely deviatoric operator H_{ijkl} having six anisotropy parameters F, G, H, L, M, and N. The parameters a and b govern

the nonlinearity of the kinematic and isotropic hardening, respectively. Note that a huge number of equivalent stresses have been proposed in the literature in order to better describe initial and induced anisotropies [34,35,39,54–60]. Note that in the context of the non-associative normality rule, the equivalent stresses in plastic potential and yield criterion are not the same [17,61–66]. This last assumption gives an important freedom to better describe plastic anisotropy, but this induces a more important number of material parameters. For example, in [17], the same Hill [38] equivalent stresses have been used, but with two different anisotropic operators giving 12 material parameters instead of 6 parameters in the present case. For the sake of simplicity and to make easy the parametric study, in this paper we limit ourselves to non-associative plasticity theory, but with the associative normality rule by taking the same stress norm as in Eqs. (6) and (7).

By applying the well-known normality rule, the following flux variables, which define the evolution of the dissipative phenomena, can be easily derived [48,51,53]:

$$D_{ij}^{\mathrm{p}} = \dot{\lambda}\frac{\partial \mathrm{F}}{\partial \sigma_{ij}} = \dot{\lambda}\frac{H_{ijkl}(\sigma_{kl}^{\mathrm{D}} - X_{kl})}{\|\underline{\sigma} - \underline{X}\|_H} = \dot{\lambda} n_{ij}^{\mathrm{p}} \quad \text{with } n_{ij}^{\mathrm{p}} = \frac{H_{ijkl}(\sigma_{kl}^{\mathrm{D}} - X_{kl})}{\|\underline{\sigma} - \underline{X}\|} \tag{8}$$

$$\dot{\alpha}_{ij} = -\dot{\lambda}\frac{\partial \mathrm{F}}{\partial X_{ij}} = \dot{\lambda}\left(n_{ij}^{\mathrm{p}} - a\alpha_{ij}\right) = D_{ij}^{\mathrm{p}} - \dot{\lambda}\frac{2}{3X_{\mathrm{sat}}}X_{ij} \tag{9}$$

$$\dot{r} = -\dot{\lambda}\frac{\partial \mathrm{F}}{\partial R} = \dot{\lambda}(1 - br) = \dot{\lambda}\left(1 - \frac{R}{R_{\mathrm{sat}}}\right) \tag{10}$$

where $X_{\mathrm{sat}} = C/a$ and $R_{\mathrm{sat}} = Q/b$ are asymptotic values, under simple tension, of the kinematic and isotropic internal stresses, respectively, representing the saturation of these two hardening phenomena. The plastic multiplier $\dot{\lambda}$ in Eqs. (8), (9) and (10) is determined using the consistency condition $\dot{f} = 0$ if $f = 0$, giving in final:

$$\dot{\lambda} = \frac{2\mu_{\mathrm{e}} n_{kl}^{\mathrm{p}} D_{kl}}{(2\mu_{\mathrm{e}} + \frac{2}{3}C)n_{kl}^{\mathrm{p}} n_{kl}^{\mathrm{p}} - \frac{C}{X_{\mathrm{sat}}} n_{kl}^{\mathrm{p}} X_{kl} + Q - \frac{Q}{R_{\mathrm{sat}}}R} \tag{11}$$

3. Identification methodology of plastic anisotropy parameters

Classically, the determination of the anisotropic plastic parameters F, G, H, L, M, and N is done using either Lankford or strain ratios ($r^{\psi} = \frac{\varepsilon_{22}^{\mathrm{p}\psi}}{\varepsilon_{33}^{\mathrm{p}\psi}}$ and $r^{b} = \frac{D_{22}^{\mathrm{p}}}{D_{11}^{\mathrm{p}}}$), or stress ratios ($S^{\psi} = \frac{\sigma^{\psi}}{\sigma^{0}}$) measured using several tensile tests along the direction ψ with respect to the material anisotropic directions, and equi-biaxial tensile test. Note that these two ratios cover the different anisotropies: while Lankford ratios describe plastic flow anisotropy, the stress ratios concern the yield surface anisotropy. These two different parameters are unified in the context of standard associative plasticity. However, this unification poses problems if the experimentally measured parameters reflect different anisotropies. Precisely, this fact is originally the precursor of non-associative plasticity models leading to separate plastic flow and yield stress anisotropies as can be found in [17,61–66]. Although this constitutes an important open problematic, we focus in this paper on another important identification problem. We assume that the unification of the yield surface and plastic flow anisotropies is proved.

The problem that attracts our attention is the fact that the Lankford ratios ($r^{\psi} = \frac{\varepsilon_{22}^{\mathrm{p}\psi}}{\varepsilon_{33}^{\mathrm{p}\psi}}$ and $r^{b} = \frac{\varepsilon_{22}^{\mathrm{p}}}{\varepsilon_{11}^{\mathrm{p}}}$) are experimentally measured at large plastic strains (i.e. between 20% to 50% failure strain) and used in the identification of anisotropic parameters with often neglecting their expected dependencies with respect to especially kinematic hardening.

Based on Eqs. (4), (8), and (9), without neglecting the hardening effect and considering a plane stress state, the expressions of the Lankford ratios for the case of a tensile test (with the tensile stress $\sigma_{11} = \sigma$) realized along direction ψ with respect to material anisotropic directions are given by:

$$\begin{aligned} r^{\psi} = \frac{\varepsilon_{22}^{\mathrm{p}\psi}}{\varepsilon_{33}^{\mathrm{p}\psi}} = &-\frac{[(G+H)(\sigma\cos^2\psi - X_{11}) - H(\sigma\sin^2\psi - X_{22}) - G(X_{11}+X_{22})]\sin^2\psi}{G(\sigma\cos^2\psi - X_{22}) + F(\sigma\sin^2\psi - X_{11})} \\ &- \frac{[(H+F)(\sigma\sin^2\psi - X_{22}) - H(\sigma\cos^2\psi - X_{11}) - F(X_{11}+X_{22})]\cos^2\psi}{G(\sigma\cos^2\psi - X_{22}) + F(\sigma\sin^2\psi - X_{11})} \\ &+ \frac{2N(\sigma\cos\psi\sin\psi - X_{12})\cos\psi\sin\psi}{G(\sigma\cos^2\psi - X_{22}) + F(\sigma\sin^2\psi - X_{11})} \end{aligned} \tag{12}$$

In Eq. (12), X_{ij} are the kinematic hardening components with respect to the local (R, T, N) material frame. These components can be considered with non-zero initial values, and their evolutions are obtained by combining equations (4), (8), and (9) giving:

$$\dot{X}_{ij} = \dot{\lambda}\left(\frac{2}{3}Cn_{ij}^{\mathrm{p}} - \frac{2}{3}Ca\alpha_{ij}\right) = \frac{2}{3}CD_{ij}^{\mathrm{p}} - \dot{\lambda}aX_{ij} = \frac{2}{3}CD_{ij}^{\mathrm{p}} - \dot{\lambda}C\frac{X_{ij}}{X_{\mathrm{sat}}} \tag{13}$$

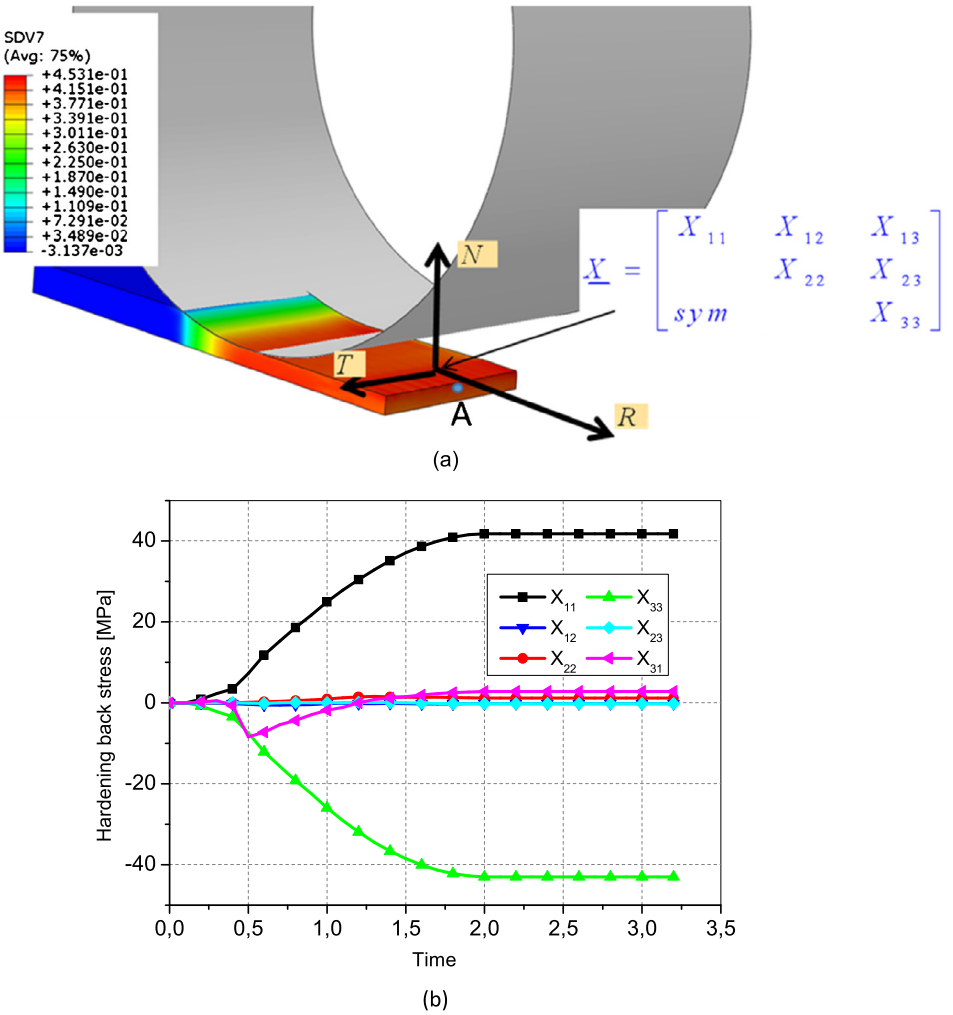

Fig. 1. An example of kinematic hardening stresses generated by the rolling process. (a) Equivalent plastic strain (kinematic hardening strain $SDV7 = \alpha_{11}$) during the rolling process. (b) Evolution of the kinematic stress tensor components during the rolling process.

Note that the initial hardening state appearing in Lankford's ratios (Eq. (12)) before plastic strain occurs is generated by prior metal forming processes, as rolling of a metallic sheet. An example of rolling process simulation for 50% thickness reduction is provided in Fig. 1. In Fig. 1a is shown the homogeneous distribution of the kinematic hardening strain α_{11} at the end of the rolling process. The temporal evolution of the kinematic hardening stress components in point A (see Fig. 1a) is drawn in Fig. 1b. From this figure, it is observed that the most significant components of the kinematic hardening tensor with respect to the rolling material frame are X_{11} and X_{33}. Accordingly, the deviatoric back stress tensor after rolling can be reduced to the following form:

$$[X_{ij}] = X_0 \begin{pmatrix} 1 & 0 & 0 \\ 0 & 0 & 0 \\ 0 & 0 & -1 \end{pmatrix} \tag{14}$$

Attention is now focused on the particular orientations $\psi = \{0°, 45°, 90°\}$, for which Eq. (12) reduces to:

$$r^0 = \frac{H(\sigma - X_{11}) + FX_{11} + (H + 2F)X_{22}}{G(\sigma - X_{22}) - FX_{11}} \tag{15}$$

$$r^{45} = \frac{N(\sigma - 2X_{12}) - (G + F)\frac{\sigma}{2} + (2G + F)X_{11} + (G + 2F)X_{22}}{G(\sigma - 2X_{22}) + F(\sigma - 2X_{11})} \tag{16}$$

$$r^{90} = \frac{H(\sigma - X_{22}) + (2G + H)X_{11} + GX_{22}}{-GX_{22} + F(\sigma - X_{11})} \tag{17}$$

It is worth noting that, when neglecting the kinematic hardening effect, Eq. (12) reduces to:

Table 2
Virtual material parameters.

E (GPa)	υ	σ_y (MPa)	C (MPa)	X_{sat} (MPa)	Q (MPa)	R_{sat} (MPa)
70	0.3	100	$100 < C < 10\,000$	$10 < X_{sat} < 100$	1000	100

Table 3
Virtual anisotropic parameters.

	F	G	H	L	M	N
Aniso1	0.20	0.40	0.60	1.00	1.00	1.00
Aniso2	0.42	0.62	0.38	2.60	2.60	2.60
Aniso3	0.74	0.55	0.45	1.23	1.23	1.23

$$r^{\psi} = \frac{\varepsilon_{22}^{p\psi}}{\varepsilon_{33}^{p\psi}} = \frac{(4H + G + F - 2N)\cos^4\psi + (2N - 4H - F - G)\cos^2\psi + H}{(G - F)\cos^2\psi + F} \tag{18}$$

When neglecting kinematic hardening in Eq. (18), the strain ratios reduce to the following well-known classical forms:

$$r^0 = \frac{H}{G}, \qquad r^{45} = \frac{N}{G + F} - \frac{1}{2}, \qquad r^{90} = \frac{H}{F} \tag{19}$$

4. Parametric study of the effect of the kinematic hardening parameters on strain ratio evolution

This investigation aims to analyze the effect of kinematic hardening on Lankford's ratios based on the use of the virtual values of material parameters defined in Tables 2 and 3. Typical evolutions of the kinematic back stresses versus the equivalent plastic strain predicted by the model using these virtual parameters are shown in Figs. 2b and 2c. The three anisotropy parameters of Table 3 are chosen such as to obtain a strain ratio greater than $r_{iso}^{\psi} = 1$ for Aniso1, less than $r_{iso}^{\psi} = 1$ for Aniso3 and oscillating around $r_{iso}^{\psi} = 1$ for Aniso2, as shown in Fig. 2a. These evolutions reflect a strong initial anisotropy for zero plastic strain according to Eqs. (15) and (16).

In this parametric study, we analyze the sensitivity of the material's response to the following parameters:

- kinematic hardening modulus C: 100 (MPa) $< C <$ 10 000 (MPa),
- saturated stress level X_{sat}: 10 (MPa) $< X_{sat} <$ 300 (MPa),
- kinematic hardening fraction $\%X$: $0\% \leq \%X = X_{sat}/(X_{sat} + R_{sat}) \leq 100\%$,
- initial kinematic hardening fraction $\%X_0$: $0 \leq \%X_0 = (X_0/X_{sat}) \leq 10\%$.

The lower and upper bounds for these parameters are chosen in such a manner that the targeted phenomena (anisotropy, Lankford's ratios variation) are significantly exhibited. Indeed, the evolutions of Lankford's ratio versus ε_{eq}^{p} and ψ according to Eq. (12) for the three considered anisotropies for the kinematic hardening fraction $\%X$ are given in Figs. 3 to 5. In these figures are provided the evolutions of Lankford's ratios with respect to plastic strain and material orientation ψ as well as their dependencies on kinematic hardening parameters for Aniso1 (Fig. 3), Aniso2 (Fig. 4), and Aniso3 (Fig. 5). These figures clearly show an increasing effect of the kinematic hardening fraction on the evolution of Lankford's ratios as the parameter $\%X$ increases. Indeed, for $\%X = 0\%$, no effect is observed on the evolution of Lankford's ratios, which remains constant when the plastic strain increases as expected from Eq. (15). The effect remains small when the kinematic hardening amount is small (case $\%X = 5\%$ or even $\%X = 50\%$ in Figs. 3b, 4b, and 5b), leading to justify the classical assumption of constant Lankford ratios. However, when the kinematic hardening amount is high ($\%X = 95\%$), significant changes of the Lankford ratios evolution are observed (Figs. 3c, 4c, and 5c).

The effect of the kinematic hardening modulus C on the Lankford ratios is depicted in Figs. 6–8 for a fixed proportion of kinematic hardening ($\%X = 50\%$). The increase of the kinematic hardening modulus C leads to an increase in the slope of Lankford ratios evolution. For example, for Aniso1 (Fig. 6) when $C = 100$ MPa, the decrease of r^{90} (maximum) is quasilinear between 3.0 and 2.7 (Fig. 6a) for an equivalent plastic strain of 33%, while for $C = 10{,}000$ MPa this decrease is observed between 3.0 and 2.0 (Fig. 6c) for an equivalent plastic strain of about 9%. However, for Aniso3 (Fig. 8) when $C = 100$ MPa, r^{45} (maximum) increases slightly between 0.45 and 0.49 (Fig. 8a) for an equivalent plastic strain of 33%, while for $C =$ 10,000 MPa, r^{45} increases abruptly between 0.45 and 0.65 (Fig. 8c) for an equivalent plastic strain of about 9%.

The parameter X_{sat} plays a similar role as that of $\%X$, and defines also the saturation level of the Lankford ratios, as can be remarked from Figs. 9–11. As shown by these figures, when X_{sat} increases, the evolution of the Lankford ratio increases, and its saturation is reached for greater plastic strain values.

Finally, the initial state of kinematic hardening, described by the parameter $\%X_0$, leads to an important increase of Lankford ratios near zero plastic strain (see Figs. 12–14). Due to the form of the initial state of kinematic hardening (see Fig. 1), Lankford's ratios mainly increase in the transverse orientation according to the rolling direction (i.e. for orientations $45° \leq \psi \leq 90°$).

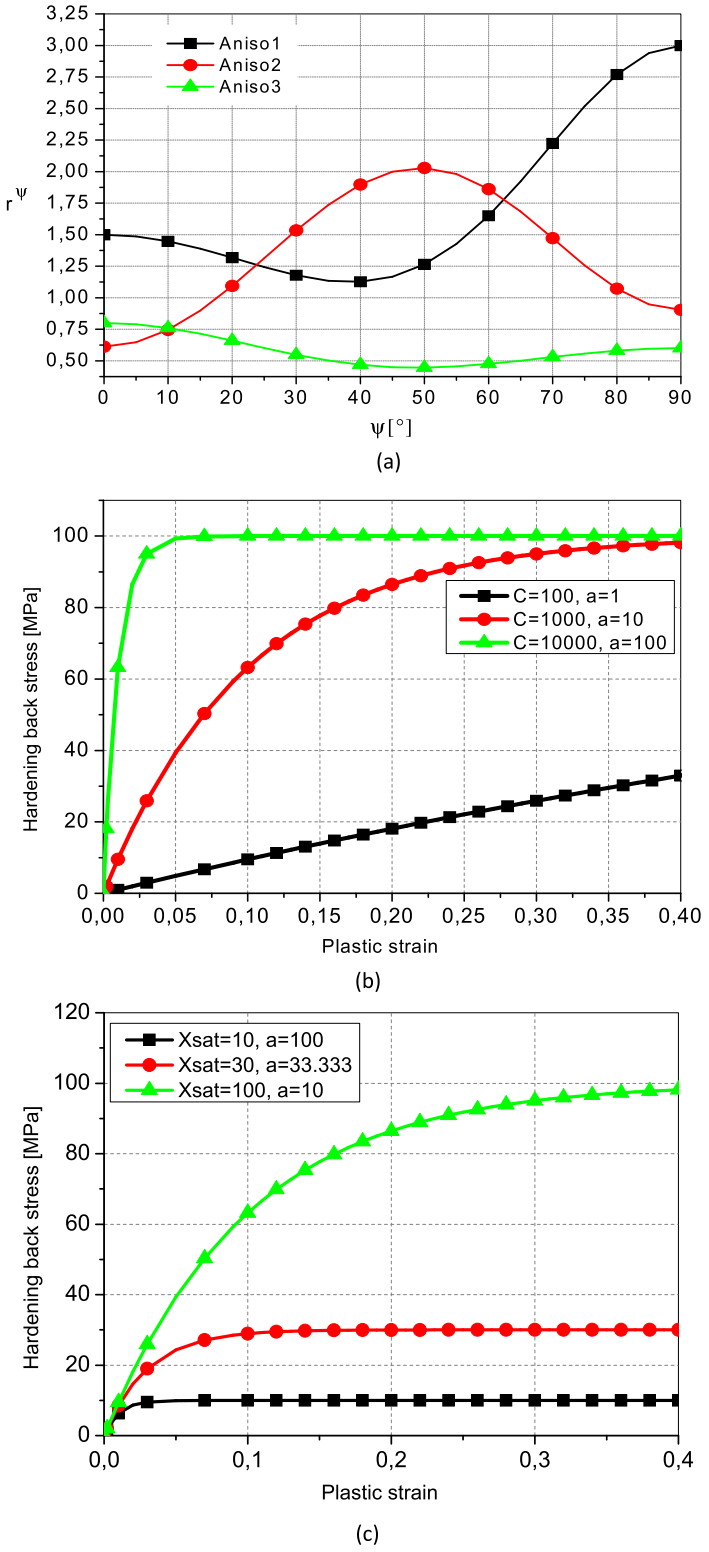

Fig. 2. Responses of the model using the virtual values of the material parameters in Table 2. (a) Strain ratios evolutions according to material orientation ψ of the three considered anisotropies for zero plastic strain ($\varepsilon^{p}_{eq} = 0$). (b) Effect of varying parameter C on the evolution of the kinematic hardening back stress according to the plastic strain with fixed saturated value $X_{sat} = 100$ MPa. (c) Effect of varying parameter X_{sat} on the evolution of the kinematic hardening back stress according to the plastic strain with fixed parameter $C = 1000$ MPa.

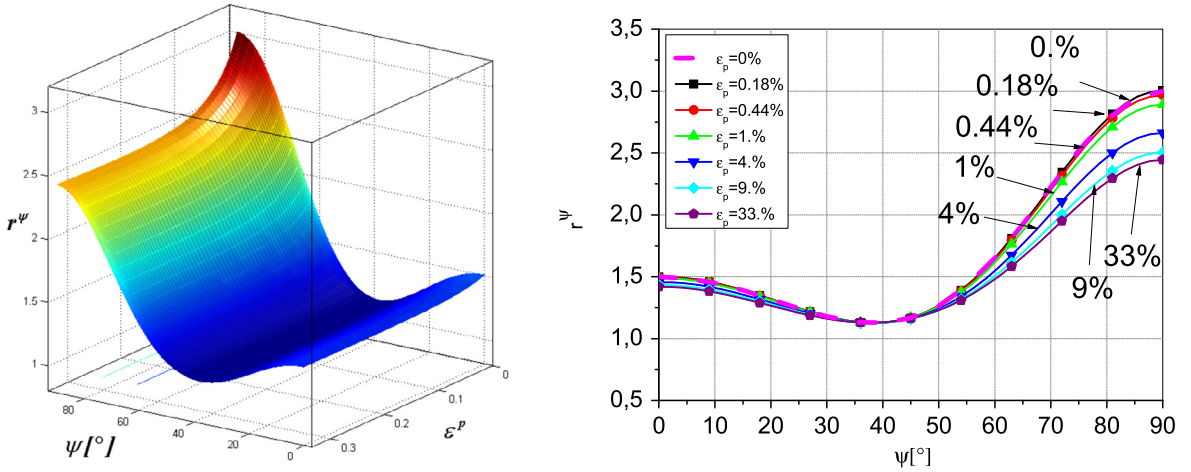

(a) %X=5%

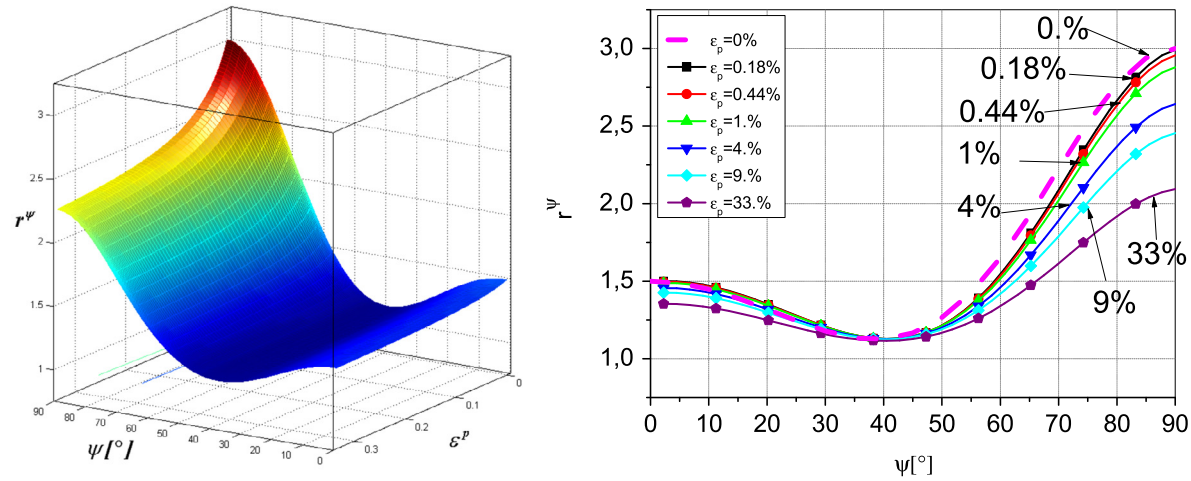

(b) %X=50%

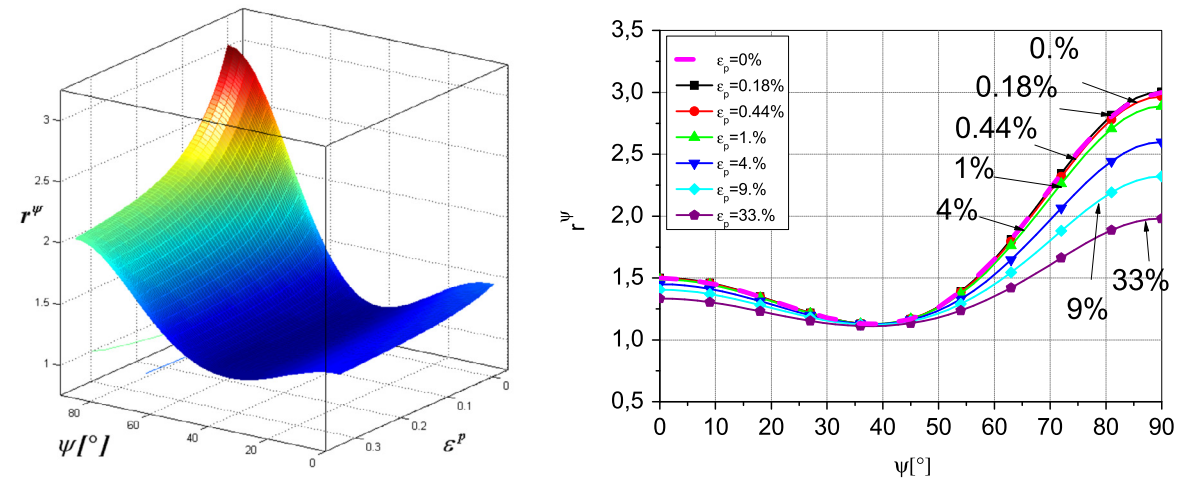

(c) %X=95%

Fig. 3. Effect of the kinematic hardening fraction $\%X$ on the evolution of r^{ψ} for the Aniso1 case with taking constant the remaining parameters $C =$ 1000 MPa, $X_{\text{sat}} = 100$ MPa, and $\%X_0 = 0\%$.

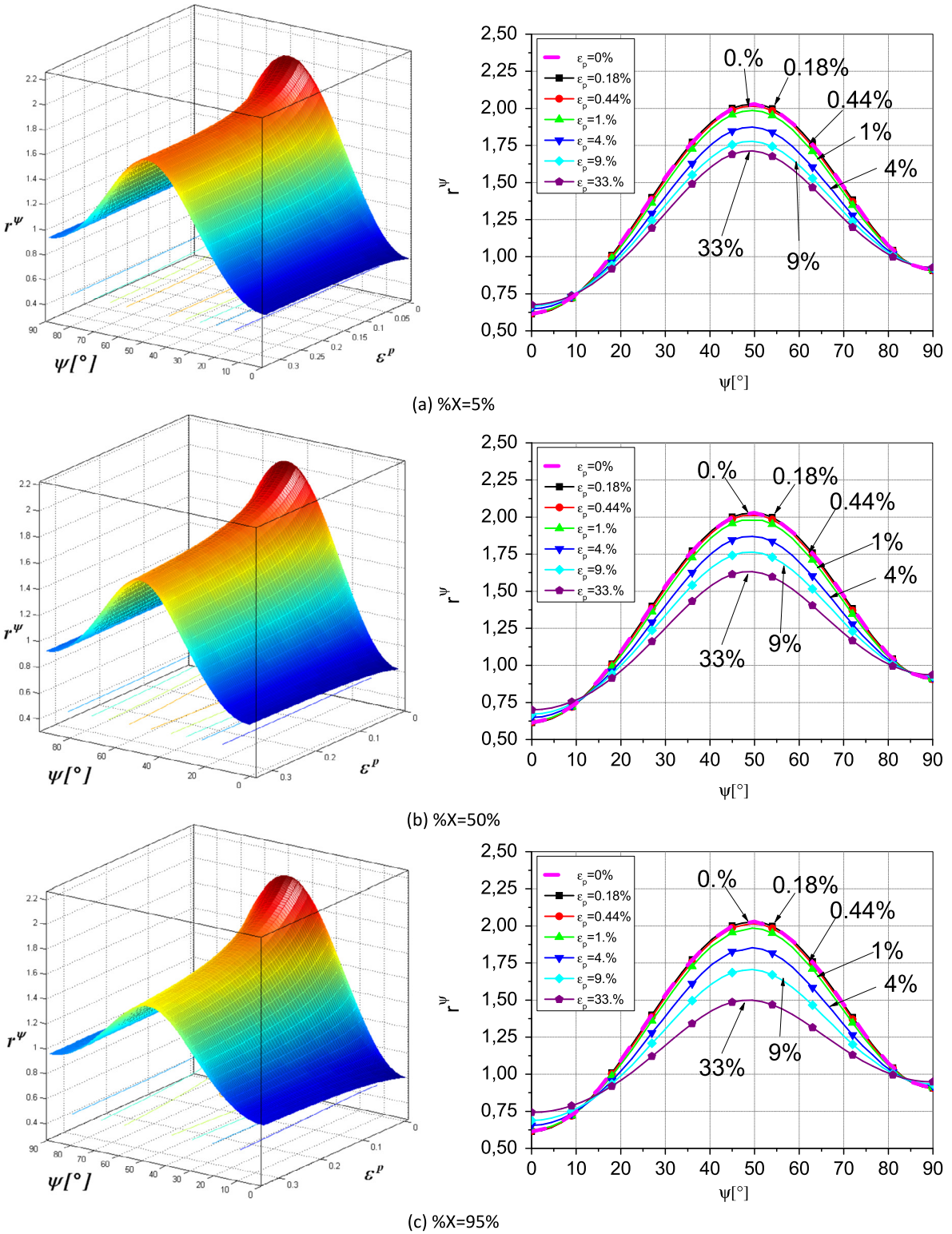

(a) %X=5%

(b) %X=50%

(c) %X=95%

Fig. 4. Effect of the kinematic hardening fraction $\%X$ on the evolution of r^{ψ} for the Aniso2 case with taking constant the remaining parameters $C =$ 1000 MPa, $X_{sat} = 100$ MPa, and $\%X_0 = 0\%$.

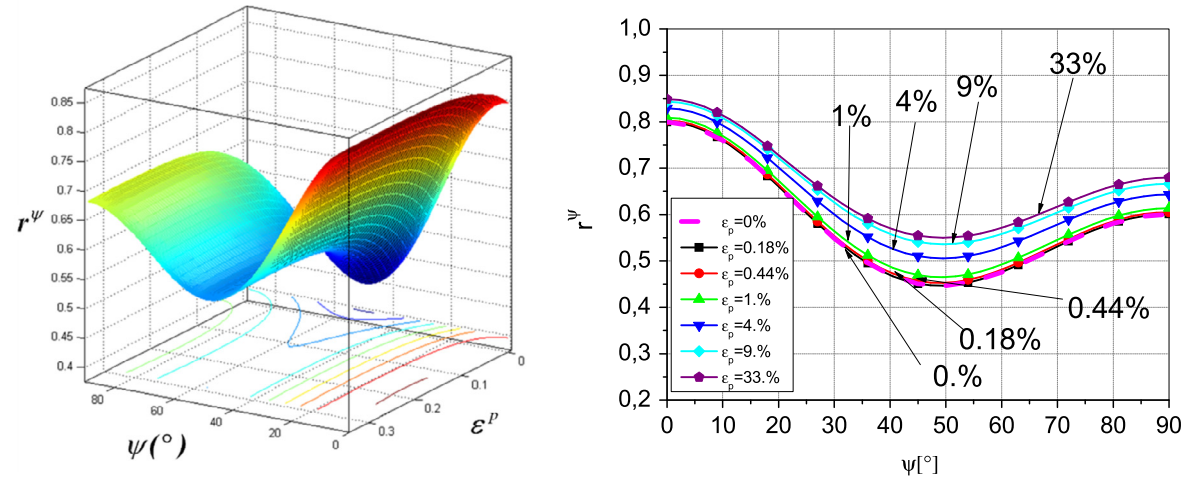

(a) %X = 5%

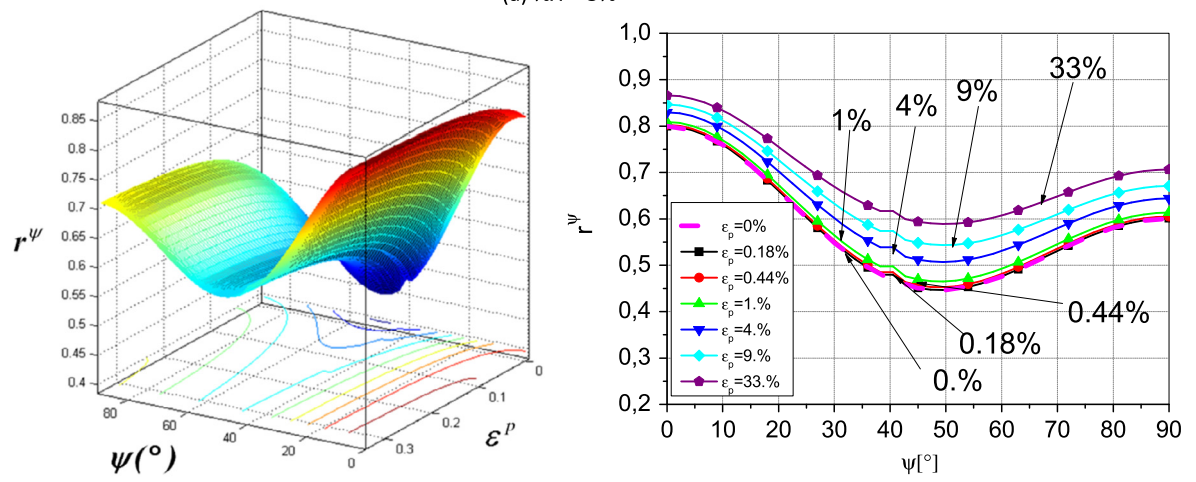

(b) %X = 50%

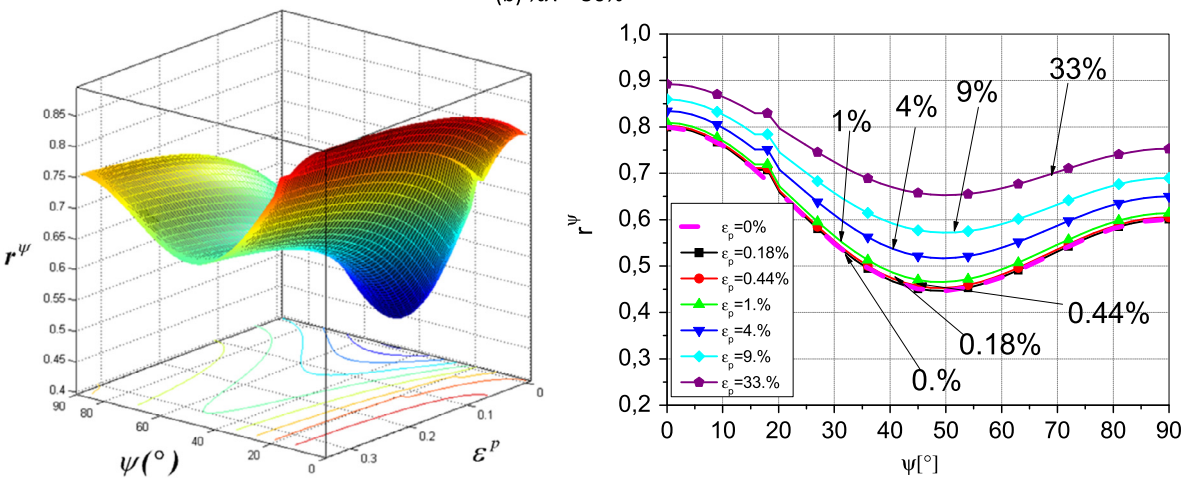

(c) %X = 95%

Fig. 5. Effect of the kinematic hardening fraction %X on the evolution of r^{ψ} for the Aniso3 case with taking constant the remaining parameters $C =$ 1000 MPa, $X_{\text{sat}} = 100$ MPa and $\%X_0 = 0\%$.

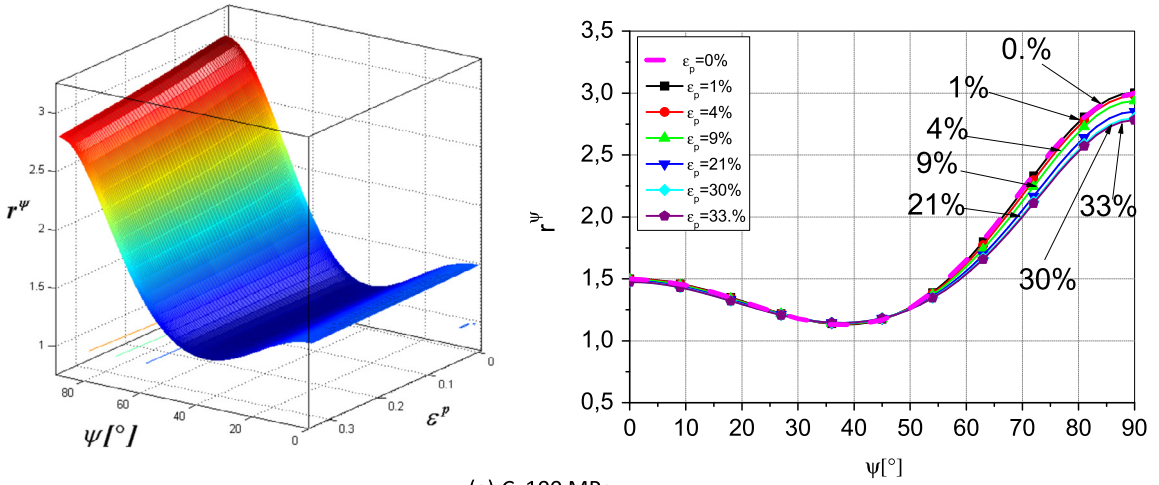

(a) C=100 MPa

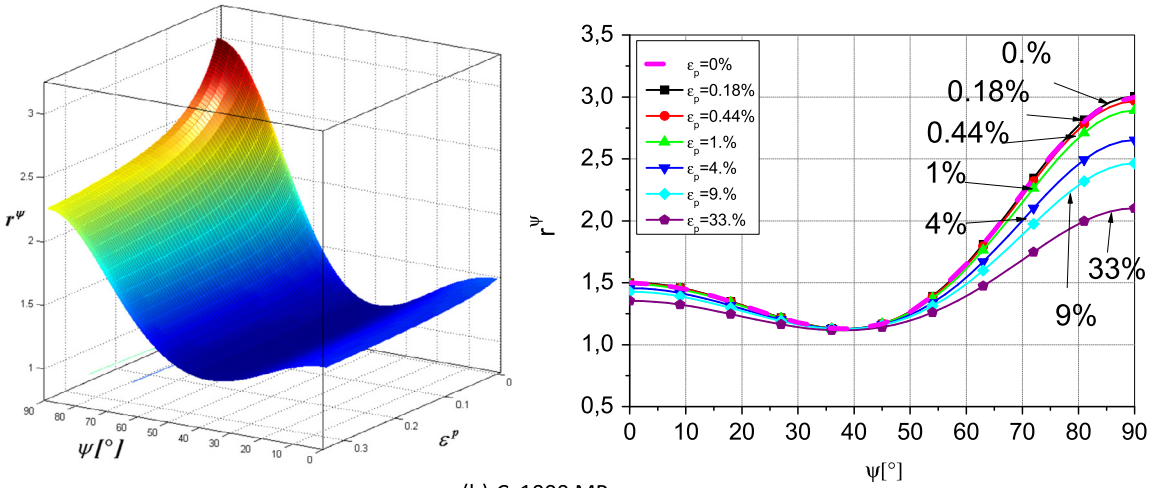

(b) C=1000 MPa

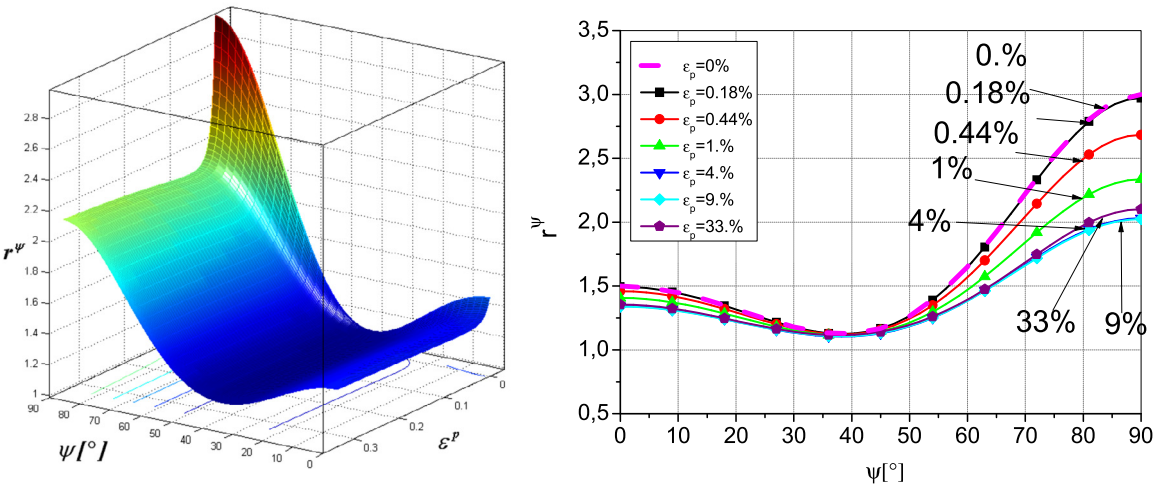

(c) C=10 000 MPa

Fig. 6. Effect of the kinematic hardening modulus C on the evolution of r^ψ for the Aniso1 case with taking constant the remaining parameters X_{sat} = 100 MPa, $\%X = 50\%$, and $\%X_0 = 0\%$.

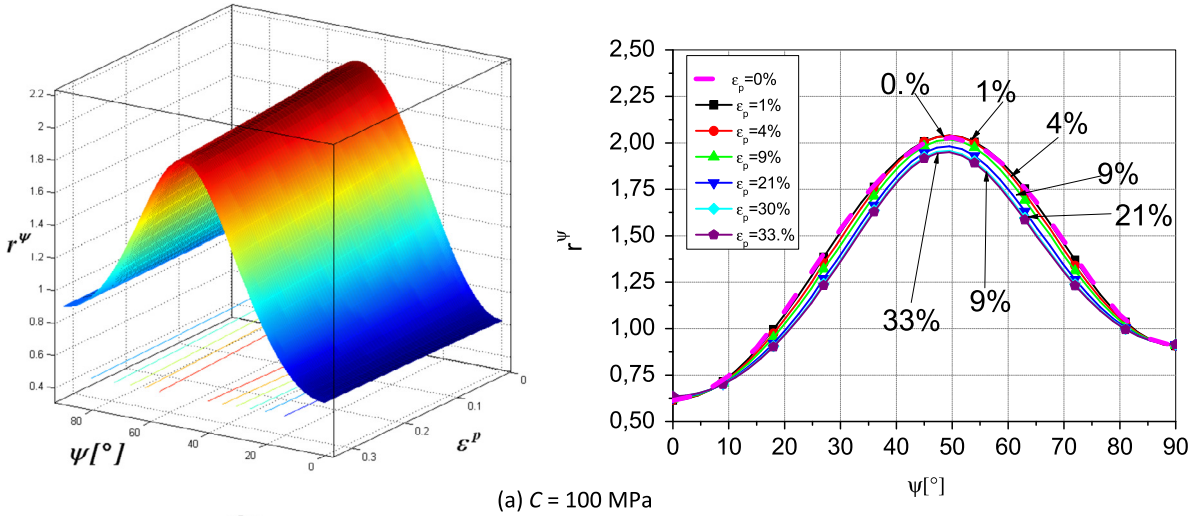

(a) C = 100 MPa

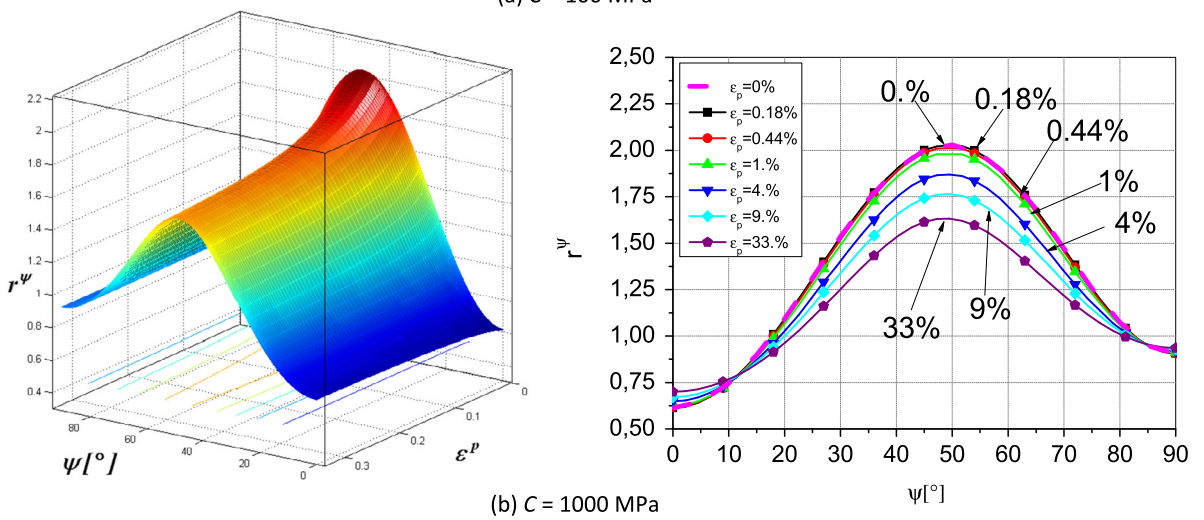

(b) C = 1000 MPa

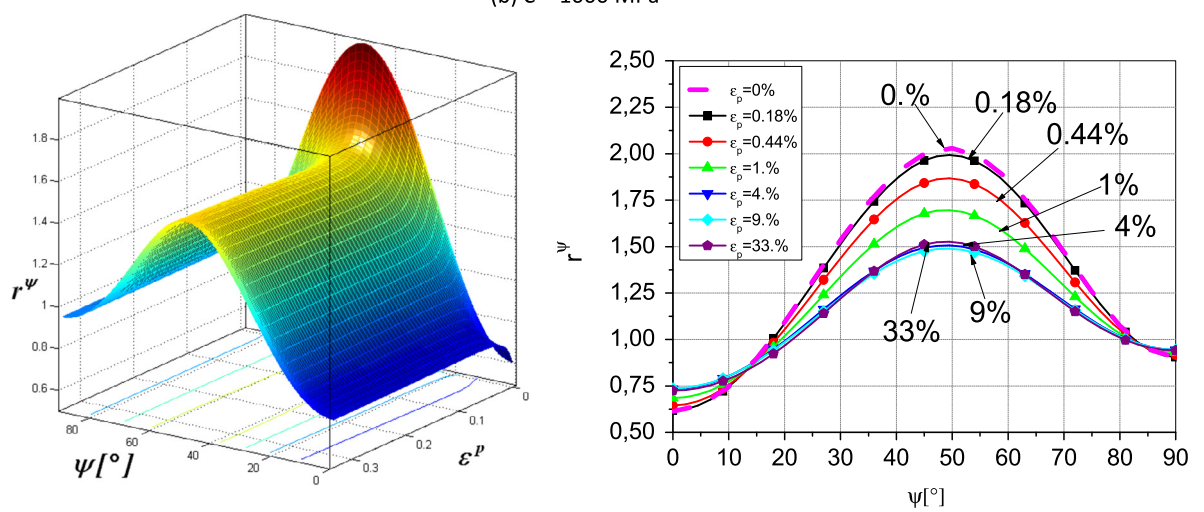

(c) C = 10 000 MPa

Fig. 7. Effect of the kinematic hardening parameter C on the evolution of r^{ψ} for the Aniso2 case with taking constant the remaining parameters $X_{\text{sat}} =$ 100 MPa, $\%X = 50\%$, and $\%X_0 = 0\%$.

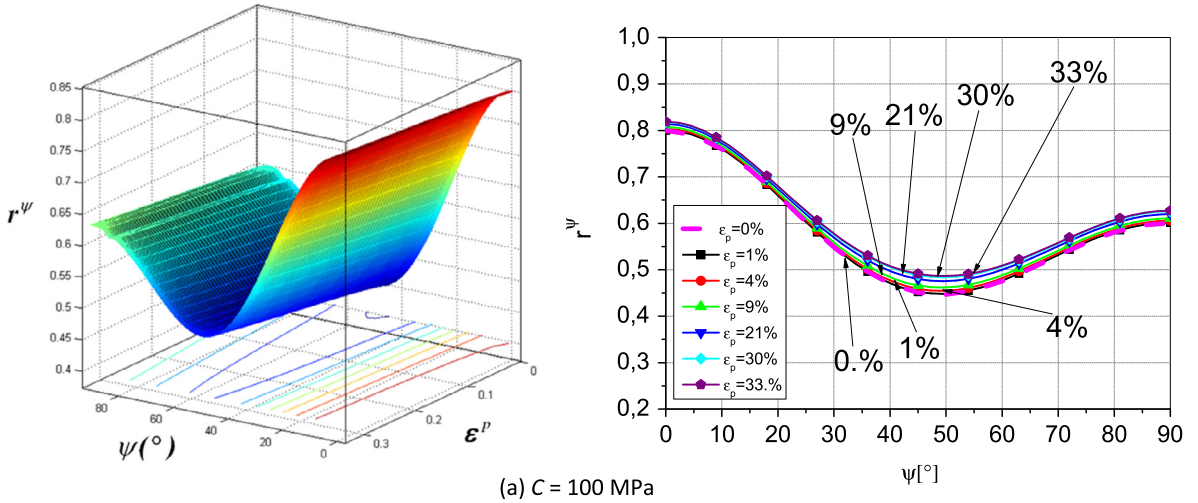

(a) C = 100 MPa

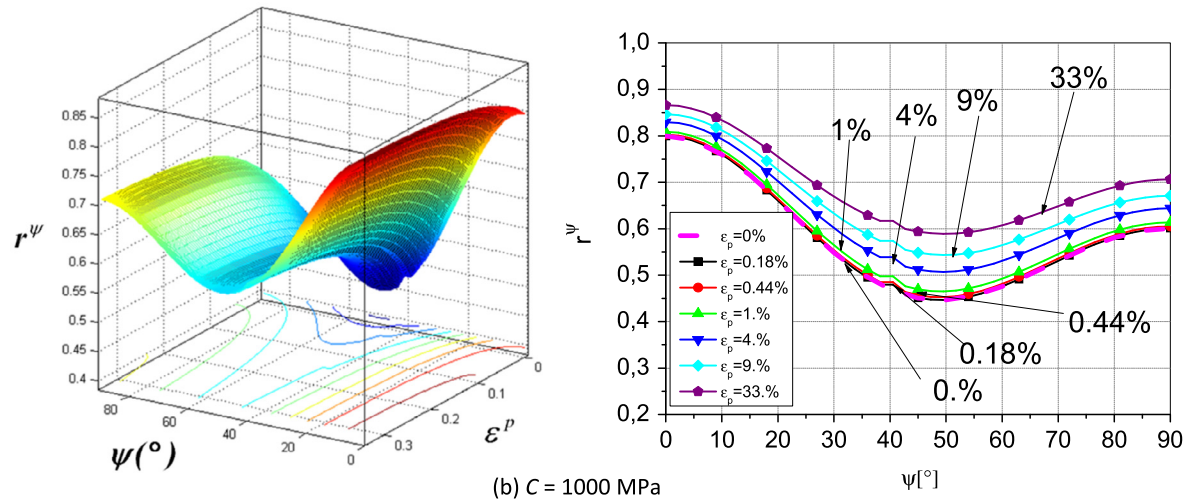

(b) C = 1000 MPa

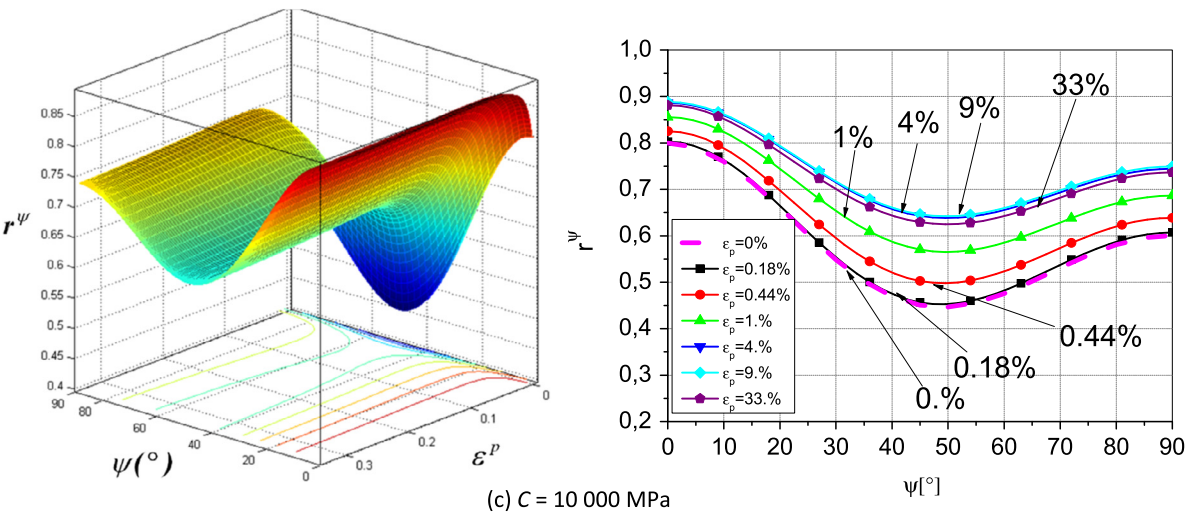

(c) C = 10 000 MPa

Fig. 8. Effect of the kinematic hardening parameter C on the evolution of r^{ψ} for the Aniso3 case with taking constant the remaining parameters X_{sat} = 100 MPa, $\%X = 50\%$, and $\%X_0 = 0\%$.

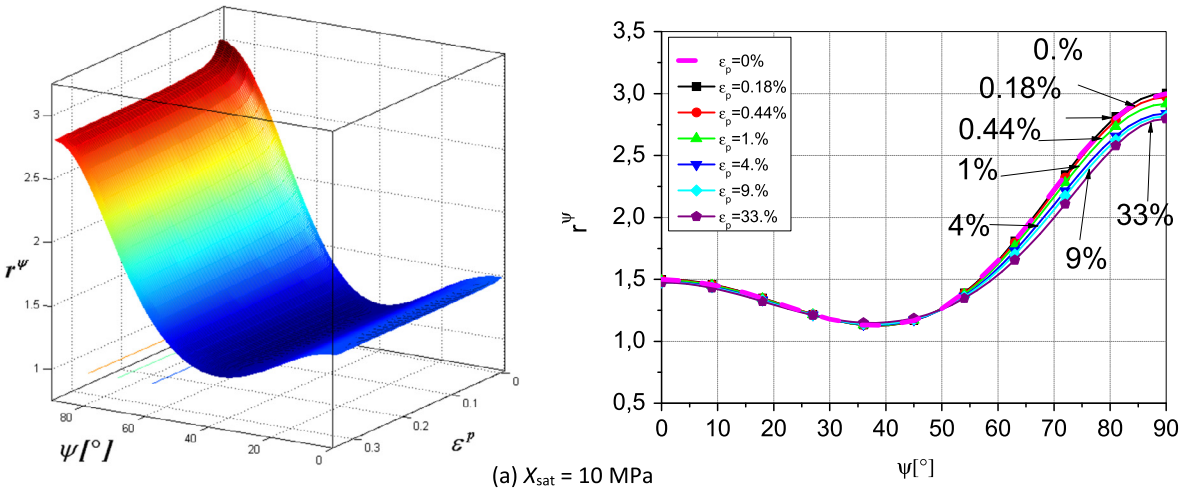

(a) X_{sat} = 10 MPa

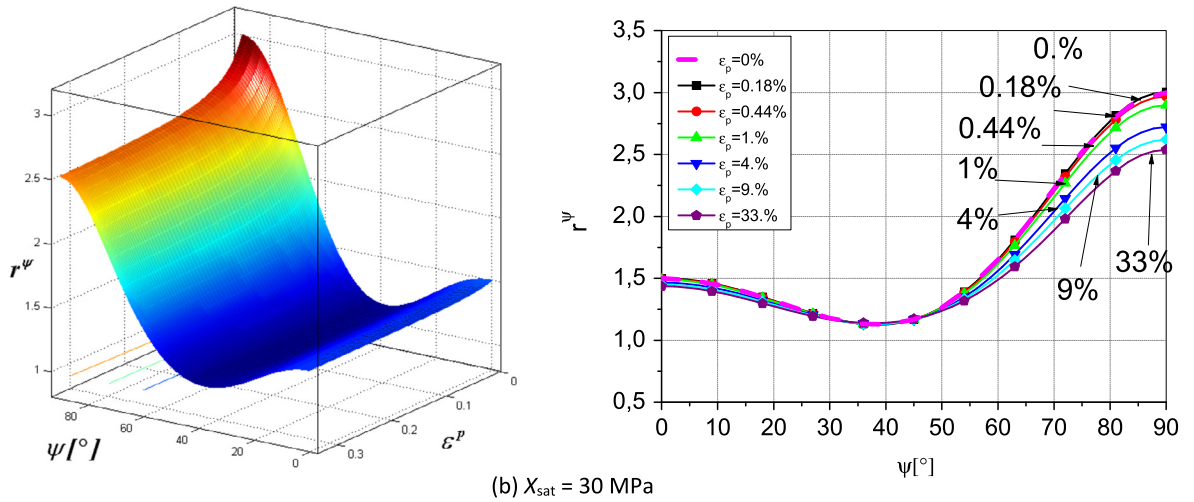

(b) X_{sat} = 30 MPa

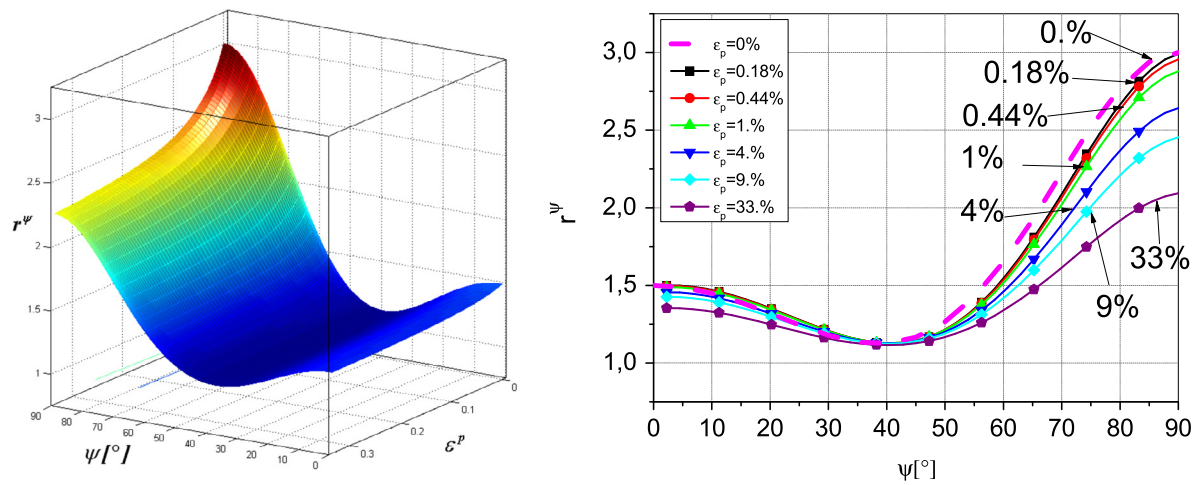

(c) X_{sat} = 100 MPa

Fig. 9. Effect of the kinematic hardening parameter X_{sat} on the evolution of r^{ψ} for the Aniso1 case with taking constant the remaining parameters $C =$ 1000 MPa, $\%X = 50\%$, and $\%X_0 = 0\%$.

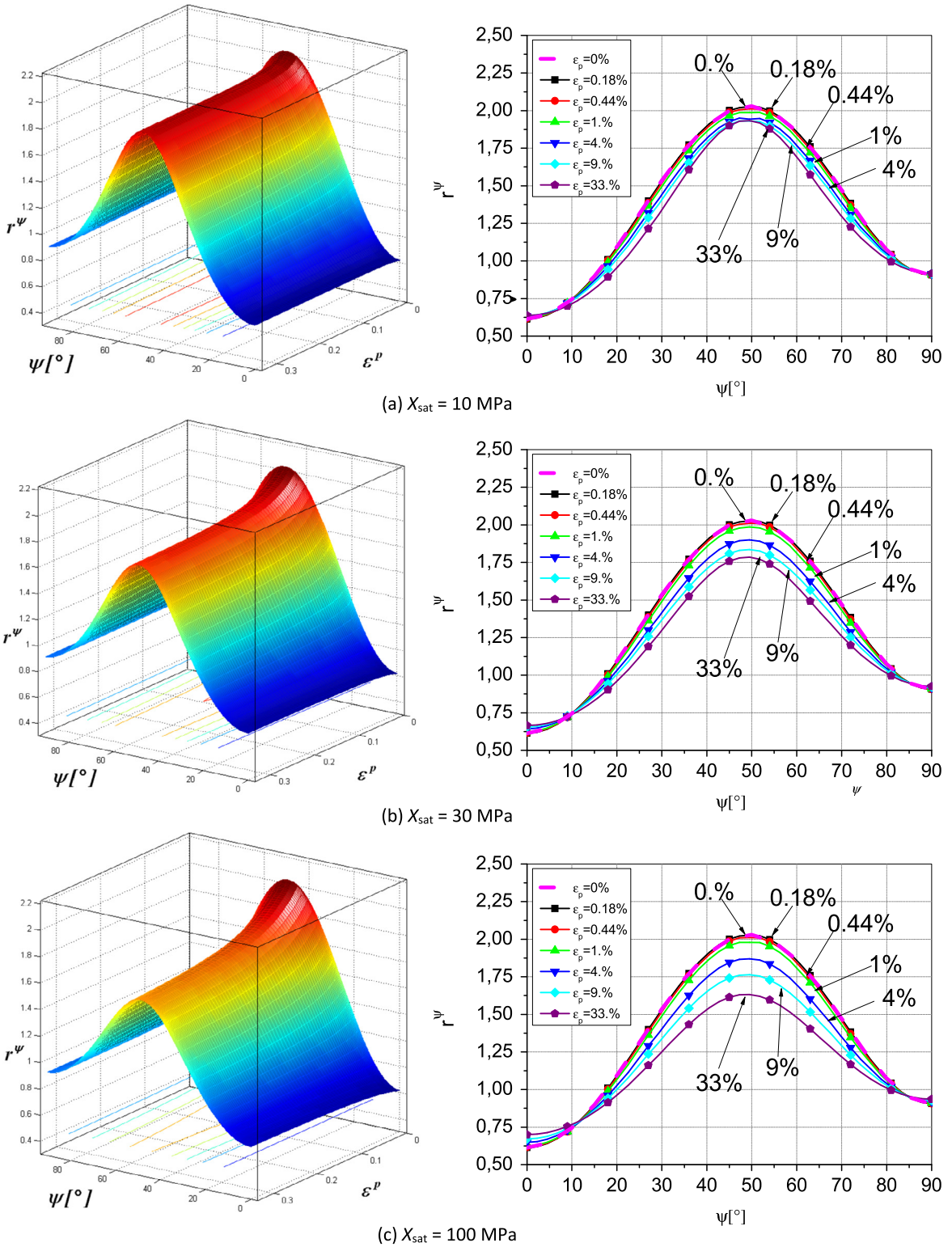

(a) X_{sat} = 10 MPa

(b) X_{sat} = 30 MPa

(c) X_{sat} = 100 MPa

Fig. 10. Effect of the kinematic hardening parameter X_{sat} on the evolution of r^{ψ} for the Aniso2 case with taking constant the remaining parameters $C = 1000$ MPa, $\%X = 50\%$, and $\%X_0 = 0\%$.

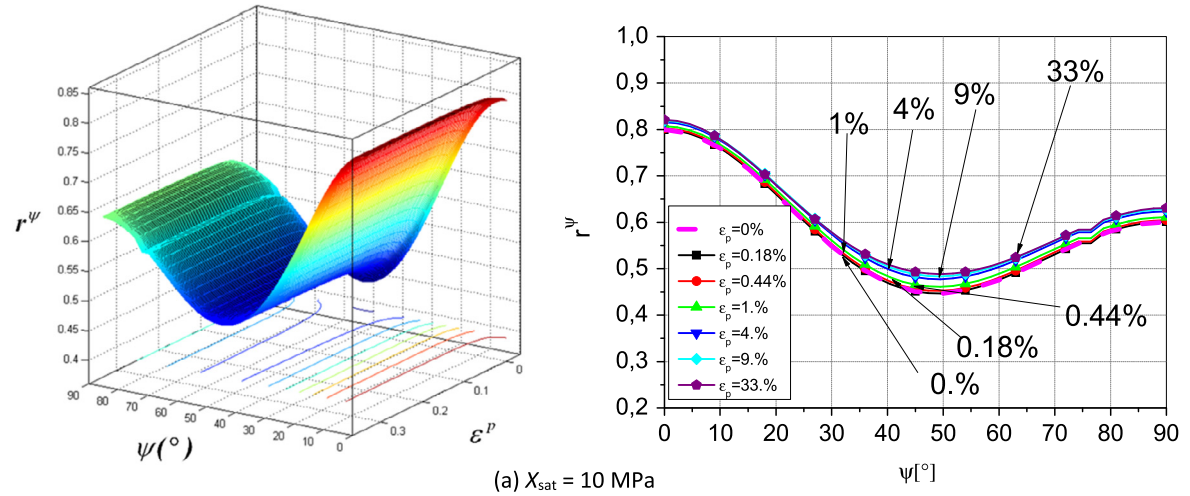

(a) X_{sat} = 10 MPa

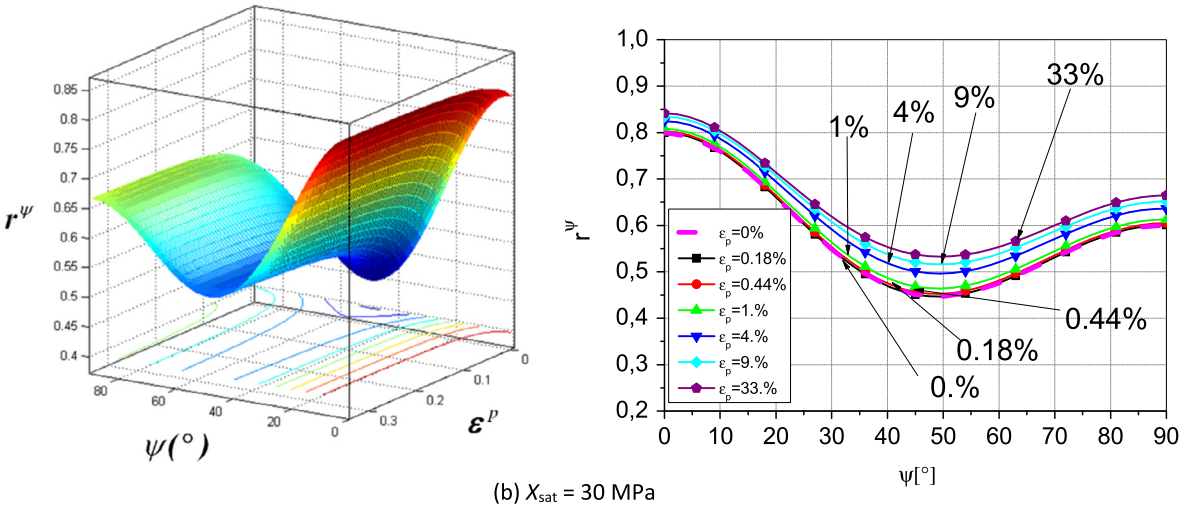

(b) X_{sat} = 30 MPa

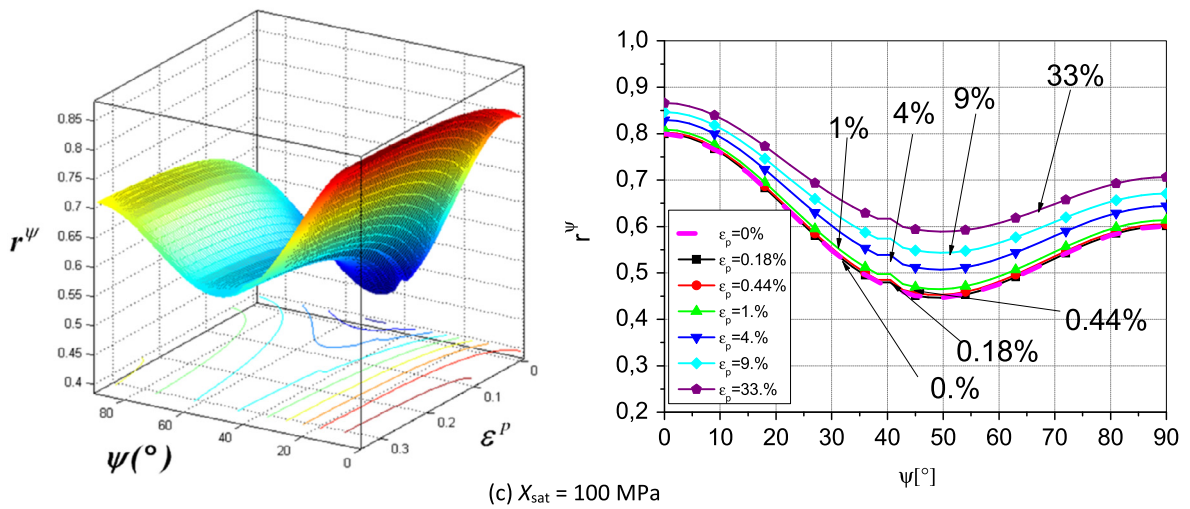

(c) X_{sat} = 100 MPa

Fig. 11. Effect of the kinematic hardening parameter X_{sat} on the evolution of r^{ψ} for the Aniso3 case with taking constant the remaining parameters $C = 1000$ MPa, $\%X = 50\%$, and $\%X_0 = 0\%$.

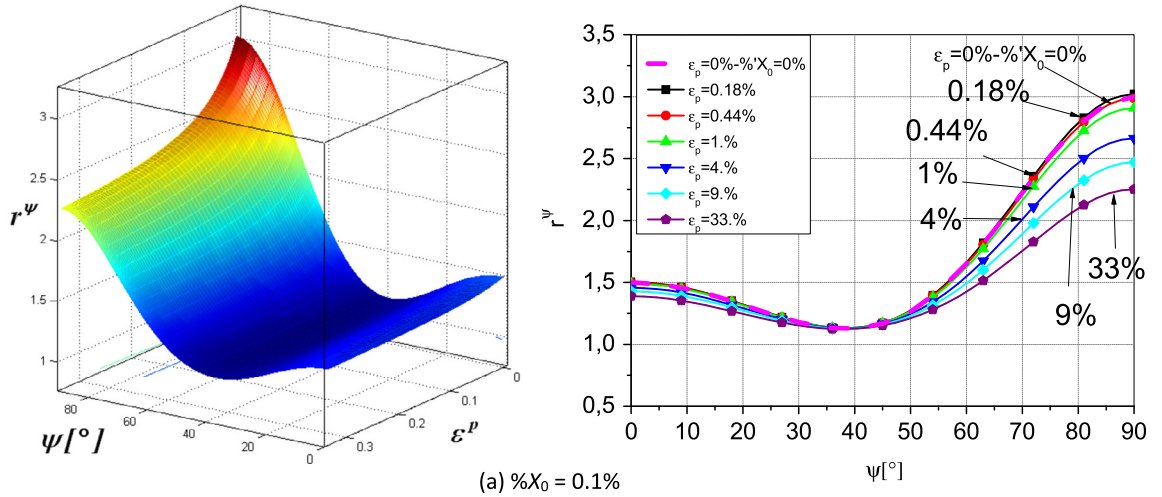

(a) %X_0 = 0.1%

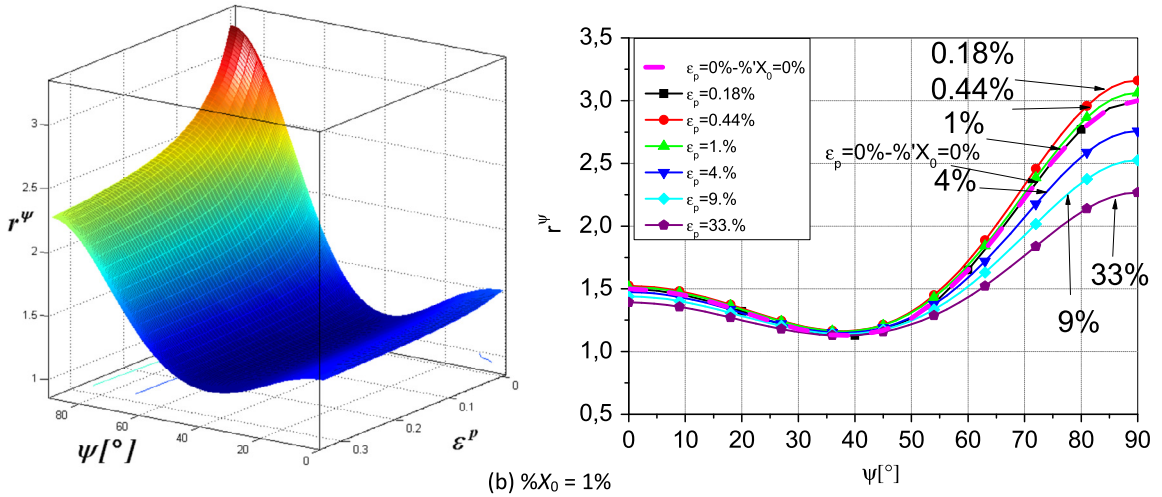

(b) %X_0 = 1%

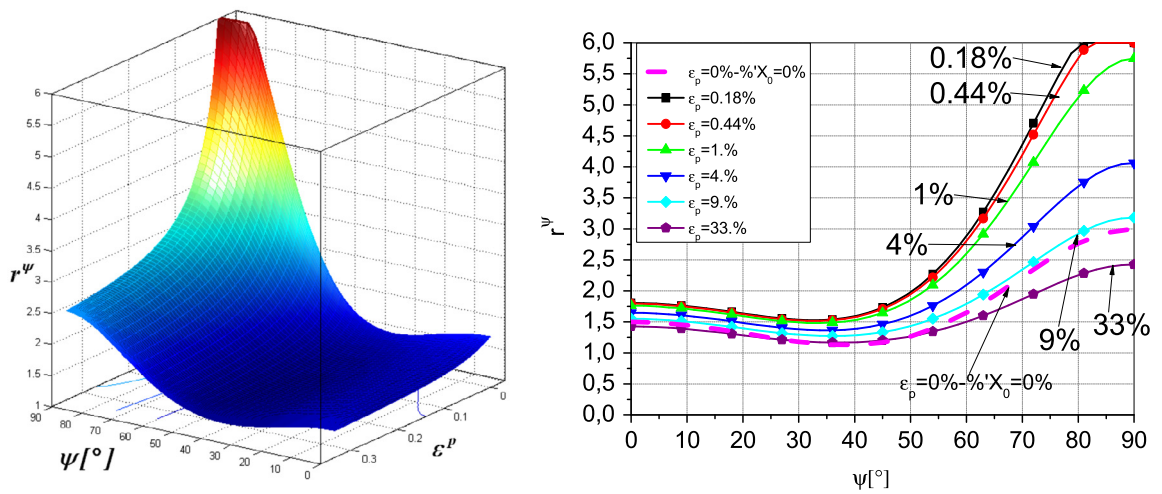

(c) %X_0 = 10%

Fig. 12. Effect of the initial kinematic hardening fraction $\%X_0$ on the evolution of r^{ψ} for the Aniso1 case with taking constant the remaining parameters $C = 1000$ MPa, $X_{\text{sat}} = 100$ MPa, and $\%X = 50\%$.

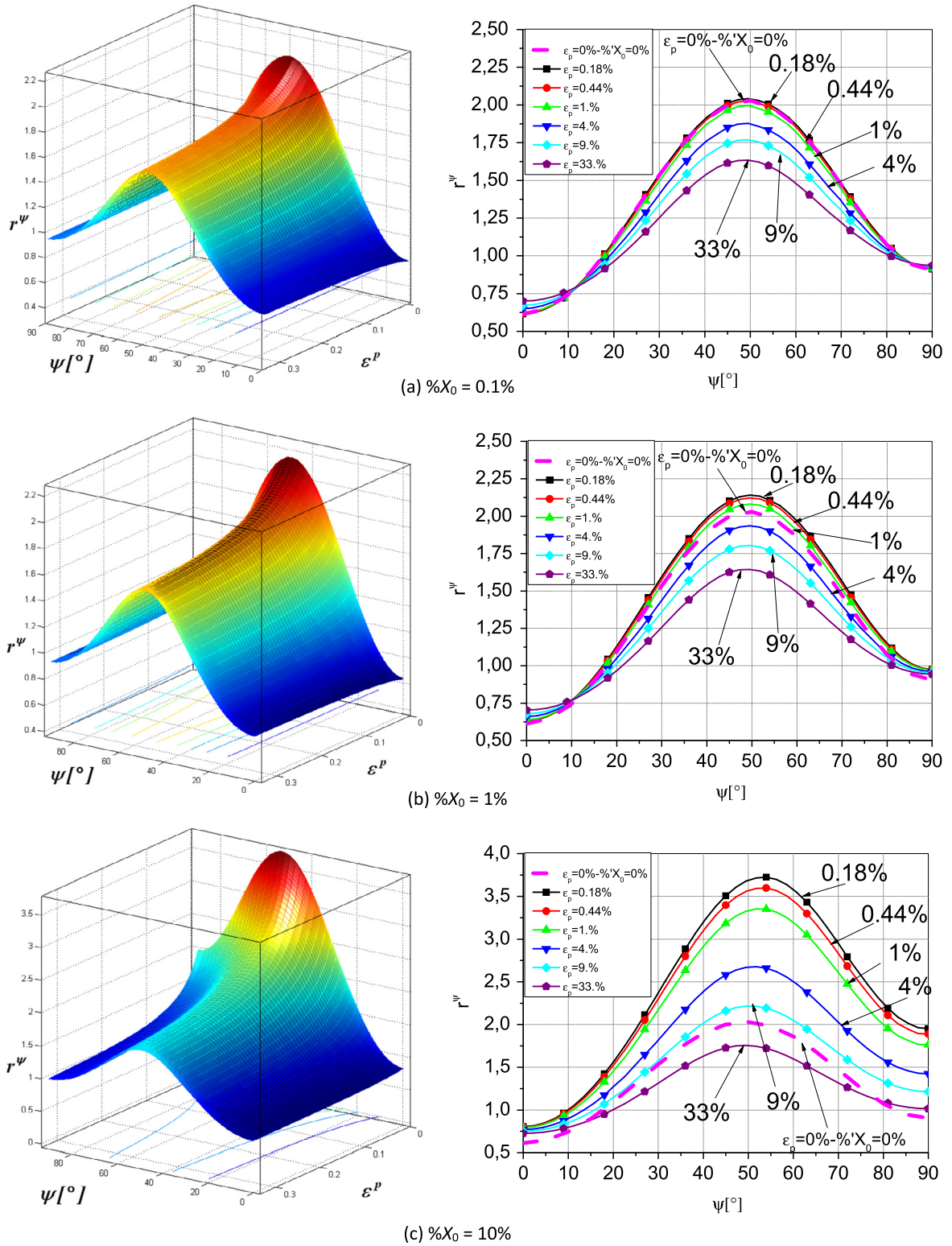

Fig. 13. Effect of the initial kinematic hardening fraction $\%X_0$ on the evolution of r^{ψ} for the Aniso2 case with taking constant the remaining parameters $C = 1000$ MPa, $X_{sat} = 100$ MPa, and $\%X = 50\%$.

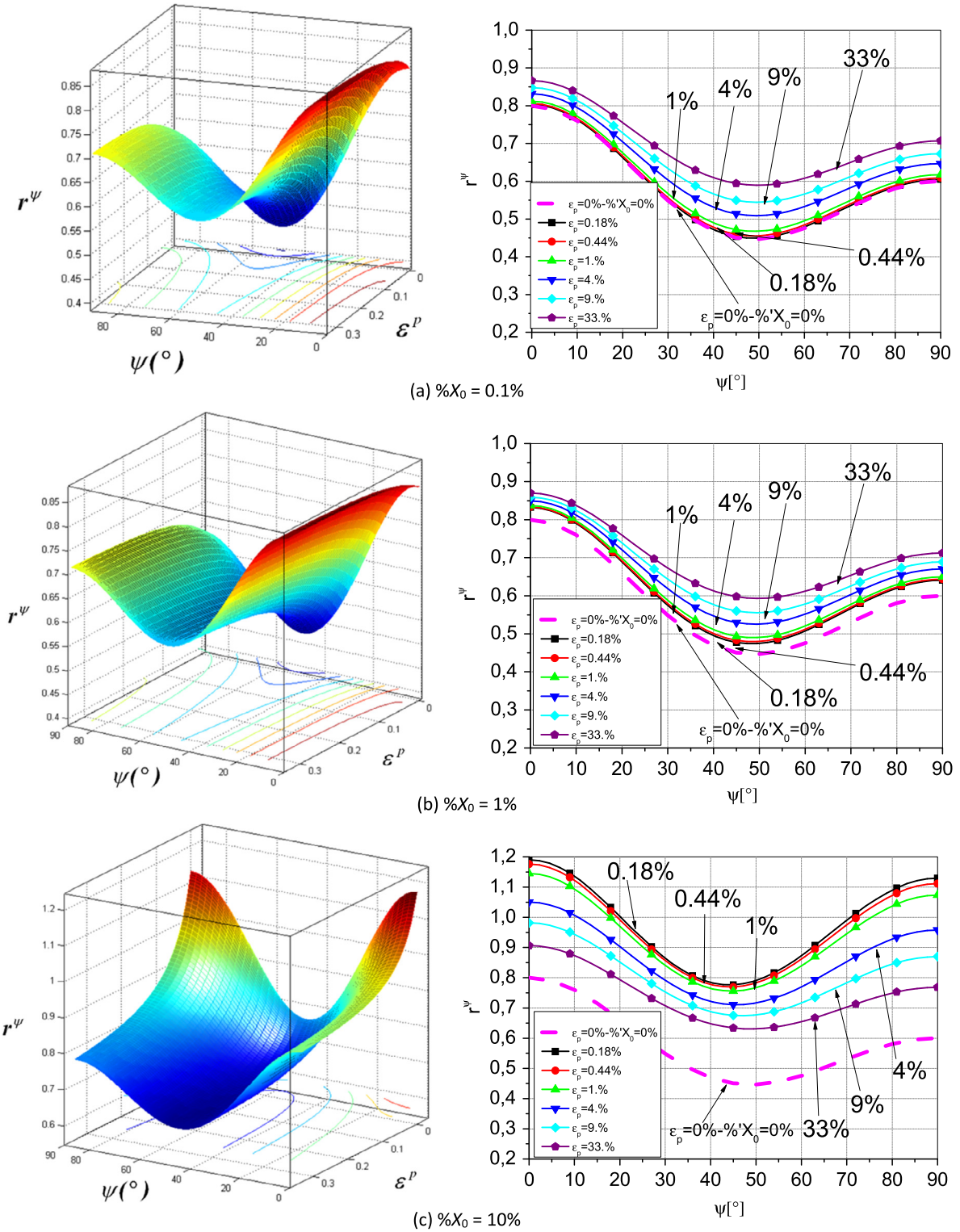

Fig. 14. Effect of the initial kinematic hardening fraction $\%X_0$ on the evolution of r^{ψ} for the Aniso3 case with taking constant the remaining parameters $C = 1000$ MPa, $X_{sat} = 100$ MPa, and $\%X = 50\%$.

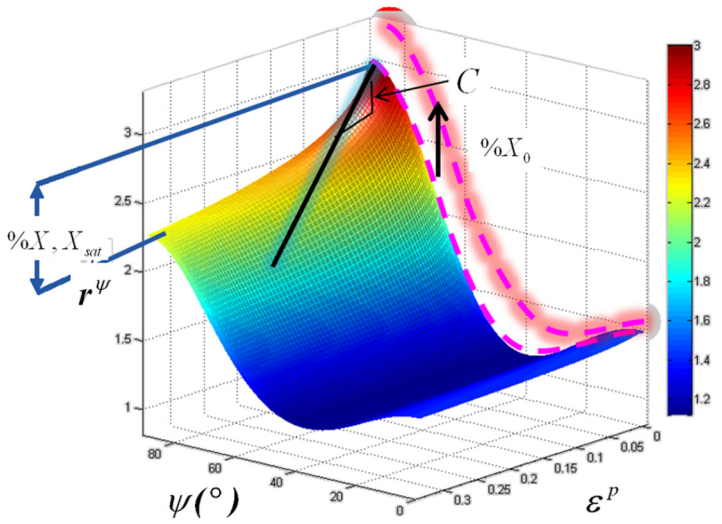

Fig. 15. Summary of the effect of the kinematic hardening parameters on the Lankford ratios.

The results of this parametric study are summarized in Fig. 15, where the effect of each kinematic hardening parameters (C, $\%X$, X_{sat}, $\%X_0$) on the evolution of Lankford's ratios is highlighted.

In the light of these results, one can conclude that accounting for kinematic hardening significantly reduces the impact of initial anisotropy, as clearly shown by the results displayed in Figs. 3–5. For Aniso1, defined by strain ratios greater than $r_{\text{iso}}^{\psi} = 1$ (see Figs. 3, 6, and 9), a decrease in the Lankford ratio mainly impacts the maximum values associated with the neighborhood of orientation $\psi = 90°$. The same tendency is observed for the case of Aniso2 (see Figs. 4, 7, and 10), for which it is observed that the decrease of the Lankford ratios mainly impacts the maximum values associated with the neighborhood of orientation $\psi = 45°$. In addition, for this case, we observe also a high increase of strain ratios having less than $r_{\text{iso}}^{\psi} = 1$ minimum values located on the neighborhood of orientation $\psi = 0°$. However, for the case of Aniso3, for which all the strain ratios values are less than $r_{\text{iso}}^{\psi} = 1$, it is observed an important increase of the values for the minimum values situated in the neighborhood of orientation $\psi = 50°$ (see Figs. 5, 8, and 11).

In Fig. 16 we displayed, for the three considered anisotropies, the sensitivity of the average Lankford ratio $\bar{r}^{\psi}$ (average relative to the orientation ψ: $\bar{r}^{\psi} = \frac{1}{90}\int_{\psi=0}^{\psi=90} r(\psi)\mathrm{d}\psi$) to kinematic hardening parameters. For the three arbitrary chosen anisotropies, it is observed that the increase of the kinematic hardening parameters ($\%X$, C, and X_{sat}) systematically induces a decrease in the average Lankford ratio for Aniso1 and Aniso2 as well as an increase for Aniso3. In Fig. 16a, we observe that an increase of the kinematic hardening modulus C leads to an increase in the average evolution of the Lankford ratios (increase for Aniso1 and Aniso2, and decrease for Aniso3). It is also observed that these evolutions reach a saturation level starting from C higher than 2000 MPa (C two times greater than the isotropic hardening modulus $Q = 1000$ MPa).

Fig. 16b shows also that the increase of the kinematic hardening saturation value X_{sat} contributes to average Lankford ratio evolution. A saturation stage starting from $X_{\text{sat}} > 200$ MPa (i.e. X_{sat} two times greater than the initial yield stress value $\sigma_y = 100$ MPa) is also observed. From Fig. 16c it is noted, as expected, that the increase of kinematic hardening amount from 0% to 100% continually induces an evolution of the average Lankford ratio, which seems to tend to the isotropic strain ratio value $r_{\text{iso}}^{\psi} = 1$.

Accordingly, it can be concluded that the evolution of kinematic hardening tends to annihilate the effect of the initial plastic anisotropy. Conversely, considering the initial state of kinematic hardening, having previous eigendirections quite different from those induced in tensile test, tends to accentuate the initial anisotropy (Fig. 16d). In this figure, we observe that when considering an initial state with 10% kinematic hardening, the average Lankford value becomes twice greater.

5. Conclusions

The main goal of this paper was to study the effect of kinematic hardening on the determination of initial anisotropy parameters. Particularly, we analyzed the effect of kinematic hardening on the Lankford ratios' evolution. This latter is often used at large plastic strain to determine the initial anisotropy parameters without taking care of its possible evolution with the increase of plastic strains. We have considered, for the sake of simplicity, a Hill [38] anisotropic plastic model in the framework of standard non-associative plasticity theory with mixed non-linear kinematic and isotropic hardenings. Through a parametric study, we have shown that accounting for kinematic hardening induces an important effect on the Lankford ratios' evolutions. We found that the evolution of kinematic hardening reduces the severity of initial anisotropy, and conversely that its initial state increases it. This suggests the need to completely review the way of the identification

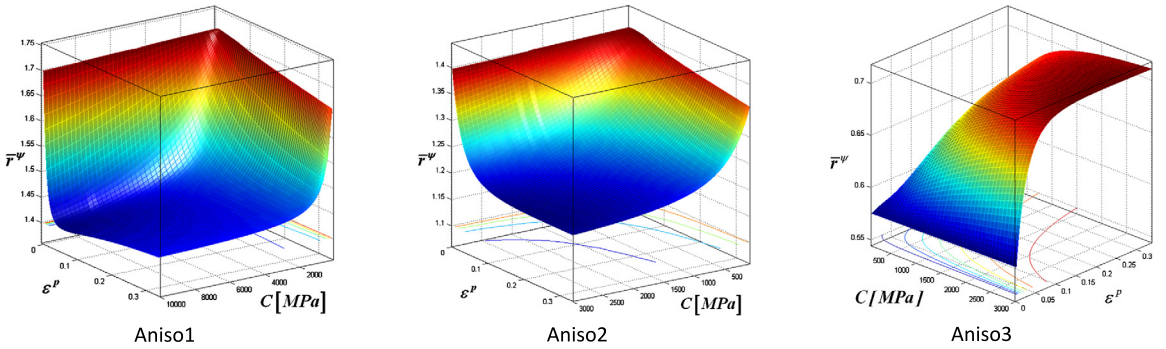

Aniso1 Aniso2 Aniso3

(a) Evolution of $\bar{r}^{\psi}$ versus C with X_{sat}=100 MPa, %X=50% and %X_0=0%

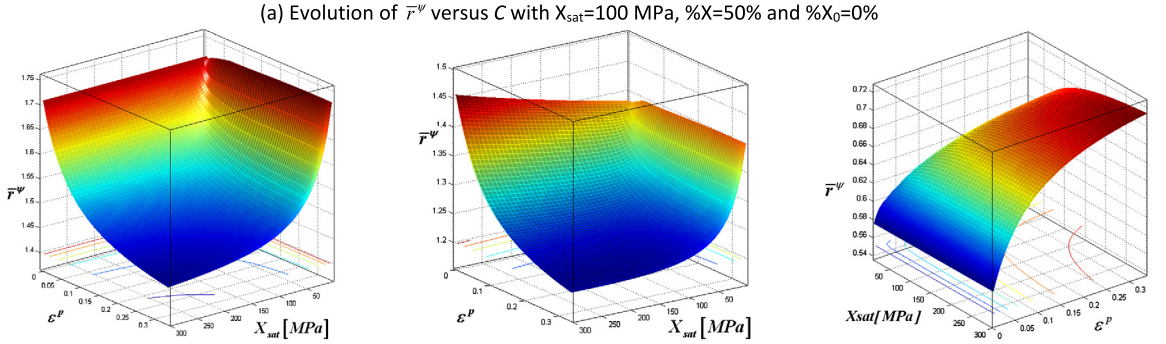

Aniso1 Aniso2 Aniso3

(b) Evolution of $\bar{r}^{\psi}$ versus X_{sat} with C = 1000 MPa, %X = 50%, and %X_0 = 0%

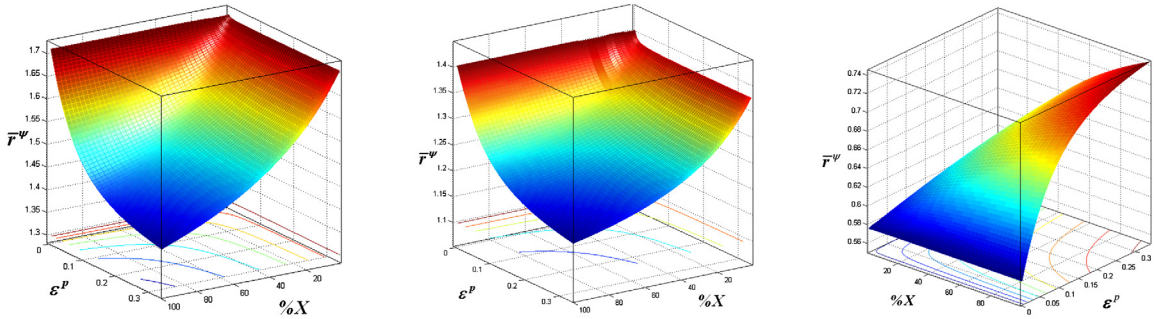

Aniso1 Aniso2 Aniso3

(c) Evolution of $\bar{r}^{\psi}$ versus %X with X_{sat} = 100, C = 1000 MPa, and %X_0 = 0%

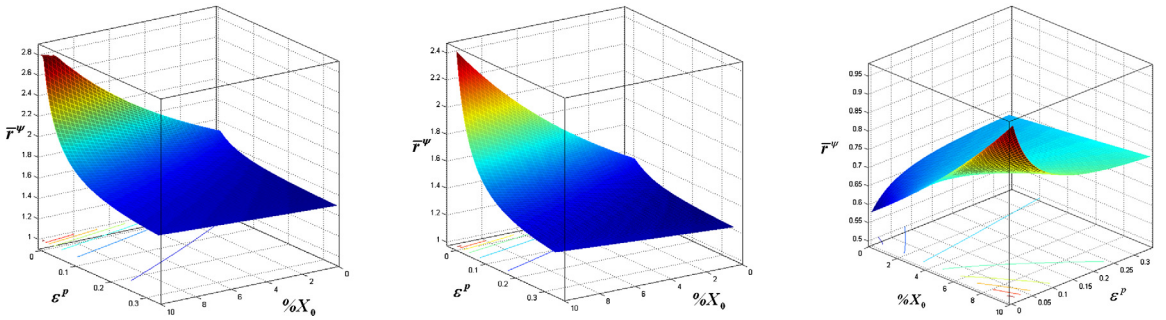

Aniso1 Aniso2 Aniso3

(d) Evolution of $\bar{r}^{\psi}$ versus %X_0 with X_{sat} = 100, C = 1000 MPa, and %X = 50%

Fig. 16. Effect of the kinematic hardening parameters on the average Lankford ratio $\bar{r}^{\psi}$.

of anisotropic parameters in the presence of kinematic hardening. The evolution of Lankford ratios with the plastic strain should be considered, and not only its singular values for particular strains.

On the other hand, this analysis on the sensitivity of the evolution of Lankford's ratio with respect to kinematic hardening parameters suggests a new way of exploring the tensile test in the identification of kinematic hardening parameters. Indeed, it is well known that the identification of the kinematic hardening parameters necessarily needs the realization of cyclic tests, usually cyclic shear tests in the case of metallic thin sheets. If we can identify the kinematic hardening parameters just by using the tensile test, this will allow considerable economy in experimental tests.

Acknowledgement

The authors gratefully acknowledge the financial support of ESI Group.

References

[1] F. Barlat, J.J. Gracio, M.-G. Lee, E.F. Rauch, G. Vincze, An alternative to kinematic hardening in classical plasticity, Int. J. Plast. 27 (2011) 1309–1327.
[2] F. Barlat, J. Ha, J.J. Grácio, M.-G. Lee, E.F. Rauch, G. Vincze, Extension of homogeneous anisotropic hardening model to cross-loading with latent effects, Int. J. Plast. 46 (2013) 130–142.
[3] K. Chung, M.-G. Lee, D. Kim, C. Kim, M.L. Wenner, F. Barlat, Spring-back evaluation of automotive sheets based on isotropic-kinematic hardening laws and non-quadratic anisotropic yield functions, part I: theory and formulation, Int. J. Plast. 21 (2005) 861–882.
[4] L. Geng, R.H. Wagoner, Role of plastic anisotropy and its evolution on springback, Int. J. Mech. Sci. 44 (2002) 123–148.
[5] B. Haddag, Contribution à la modélisation de la mise en forme des tôles métalliques: application au retour élastique et à la localisation, Arts et Métiers ParisTech, 2007.
[6] B. Haddag, T. Balan, F. Abed-Meraim, Springback simulation: impact of some advanced constitutive models and numerical parameters, in: AIP Conference Proceedings, IOP Institute of Physics Publishing Ltd., 2005, p. 286.
[7] J.-W. Lee, M.-G. Lee, F. Barlat, Finite element modeling using homogeneous anisotropic hardening and application to spring-back prediction, Int. J. Plast. 29 (2012) 13–41.
[8] J.-Y. Lee, J.-W. Lee, M.-G. Lee, F. Barlat, An application of homogeneous anisotropic hardening to springback prediction in pre-strained U-draw/bending, Int. J. Solids Struct. 49 (2012) 3562–3572.
[9] M.-G. Lee, D. Kim, C. Kim, M. Wenner, R. Wagoner, K. Chung, A practical two-surface plasticity model and its application to spring-back prediction, Int. J. Plast. 23 (2007) 1189–1212.
[10] M. Oliveira, J. Alves, B. Chaparro, L. Menezes, Study on the influence of work-hardening modeling in springback prediction, Int. J. Plast. 23 (2007) 516–543.
[11] I.N. Vladimirov, M.P. Pietryga, S. Reese, Anisotropic finite elastoplasticity with nonlinear kinematic and isotropic hardening and application to sheet metal forming, Int. J. Plast. 26 (2010) 659–687.
[12] P.J. Armstrong, C.O. Frederick, A Mathematical Representation of the Multiaxial Bauschinger Effect, Central Electricity Generating Board Report Berkeley Nuclear Laboratories, 1966.
[13] J.-L. Chaboche, Time-independent constitutive theories for cyclic plasticity, Int. J. Plast. 2 (1986) 149–188.
[14] H. Haddadi, S. Bouvier, M. Banu, C. Maier, C. Teodosiu, Towards an accurate description of the anisotropic behaviour of sheet metals under large plastic deformations: modelling, numerical analysis and identification, Int. J. Plast. 22 (2006) 2226–2271.
[15] C. Teodosiu, Z. Hu, Microstructure in the continuum modelling of plastic anisotropy, in: Nineteenth Riso International Symposium on Materials Science 1998, 1998, pp. 149–168.
[16] H. Aretz, A simple isotropic-distortional hardening model and its application in elastic–plastic analysis of localized necking in orthotropic sheet metals, Int. J. Plast. 24 (2008) 1457–1480.
[17] H. Badreddine, K. Saanouni, A. Dogui, On non-associative anisotropic finite plasticity fully coupled with isotropic ductile damage for metal forming, Int. J. Plast. 26 (2010) 1541–1575.
[18] M. Khelifa, H. Badreddine, N. Belamri, M. Gahbiche, K. Saanouni, A. Cherouat, A. Dogui, Effect of anisotropic plastic flow on the ductile damage evolution in hydrobulging test of thin sheet metal, Int. J. Form. Process. 8 (2005) 271.
[19] J. Lee, J.-Y. Lee, F. Barlat, R. Wagoner, K. Chung, M.-G. Lee, Extension of quasi-plastic–elastic approach to incorporate complex plastic flow behavior – application to springback of advanced high-strength steels, Int. J. Plast. 45 (2013) 140–159.
[20] S. Msolli, H. Badreddine, C. Labergère, M. Martiny, G. Robin, M. Jrad, K. Saanouni, F. Choquart, Experimental characterization and numerical prediction of ductile damage in forming of AA1050-O sheets, Int. J. Mech. Sci. 99 (2015) 262–273.
[21] H.-C. Wu, Anisotropic plasticity for sheet metals using the concept of combined isotropic-kinematic hardening, Int. J. Plast. 18 (2002) 1661–1682.
[22] F. Yoshida, T. Uemori, A model of large-strain cyclic plasticity describing the Bauschinger effect and workhardening stagnation, Int. J. Plast. 18 (2002) 661–686.
[23] H.P. Feigenbaum, Y.F. Dafalias, Directional distortional hardening in metal plasticity within thermodynamics, Int. J. Solids Struct. 44 (2007) 7526–7542.
[24] H.P. Feigenbaum, Y.F. Dafalias, Simple model for directional distortional hardening in metal plasticity within thermodynamics, J. Eng. Mech. 134 (2008) 730–738.
[25] H.P. Feigenbaum, Y.F. Dafalias, Directional distortional hardening at large plastic deformations, Int. J. Solids Struct. 51 (2014) 3904–3918.
[26] M. François, A plasticity model with yield surface distortion for non proportional loading, Int. J. Plast. 17 (2001) 703–717.
[27] R. Hill, S.S. Hecker, M.G. Stout, An investigation of plastic flow and differential work hardening in orthotropic brass tubes under fluid pressure and axial load, Int. J. Solids Struct. 31 (1994) 2999–3021.
[28] T. Kurtyka, M. Życzkowski, Evolution equations for distortional plastic hardening, Int. J. Plast. 12 (1996) 191–213.
[29] L. Vincent, S. Calloch, T. Kurtyka, D. Marquis, An improvement of multiaxial ratcheting modeling via yield surface distortion, J. Eng. Mater. Technol. 124 (2002) 402–411.
[30] G.Z. Voyiadjis, M. Foroozesh, Anisotropic distortional yield model, J. Appl. Mech. 57 (1990) 537–547.
[31] D. Banabic, Formability of Metallic Materials: Plastic Anisotropy, Formability Testing, Forming Limits, Springer Science & Business Media, 2000.
[32] D. Banabic, F. Barlat, O. Cazacu, T. Kuwabara, Advances in anisotropy and formability, Int. J. Form. 3 (2010) 165–189.
[33] F. Barlat, R. Becker, Y. Hayashida, Y. Maeda, M. Yanagawa, K. Chung, J. Brem, D. Lege, K. Matsui, S. Murtha, Yielding description for solution strengthened aluminum alloys, Int. J. Plast. 13 (1997) 385–401.
[34] F. Barlat, D.J. Lege, J.C. Brem, A six-component yield function for anisotropic materials, Int. J. Plast. 7 (1991) 693–712.
[35] F. Barlat, Y. Maeda, K. Chung, M. Yanagawa, J. Brem, Y. Hayashida, D. Lege, K. Matsui, S. Murtha, S. Hattori, Yield function development for aluminum alloy sheets, J. Mech. Phys. Solids 45 (1997) 1727–1763.

[36] K. Chung, S. Lee, F. Barlat, Y. Keum, J. Park, Finite element simulation of sheet forming based on a planar anisotropic strain-rate potential, Int. J. Plast. 12 (1996) 93–115.
[37] F. Habraken, J. Dautzenberg, Some applications of the Barlat 1991 yield criterion, CIRP Ann., Manuf. Technol. 44 (1995) 185–188.
[38] R. Hill, A theory of the yielding and plastic flow of anisotropic metals, Proc. R. Soc. Lond. A, Math. Phys. Eng. Sci. (1948) 281–297, The Royal Society.
[39] A. Karafillis, M. Boyce, A general anisotropic yield criterion using bounds and a transformation weighting tensor, J. Mech. Phys. Solids 41 (1993) 1859–1886.
[40] Z. Yue, H. Badreddine, T. Dang, K. Saanouni, A. Tekkaya, Formability prediction of AL7020 with experimental and numerical failure criteria, J. Mater. Process. Technol. 218 (2015) 80–88.
[41] Z. Yue, C. Soyarslan, H. Badreddine, K. Saanouni, A. Tekkaya, Identification of fully coupled anisotropic plasticity and damage constitutive equations using a hybrid experimental–numerical methodology with various triaxialities, Int. J. Damage Mech. (2014).
[42] E.H. Lee, R.L. Mallet, T.B. Wertheimer, Stress analysis for anisotropic hardening in finite-deformation plasticity, J. Appl. Mech. 50 (1983) 554–560.
[43] J. Mandel, Équations constitutives et directeurs dans les milieux plastiques et viscoplastiques, Int. J. Solids Struct. 9 (1971) 725–740.
[44] J.R. Rice, Inelastic constitutive relations for solids, an internal variable theory and its application to metal plasticity, J. Mech. Phys. Solids 9 (1971) 233–244.
[45] F. Sidoroff, The geometrical concept of intermediate configuration and elastic plastic finite strain, Arch. Mech. 25 (1973) 299–308.
[46] F. Sidoroff, Incremental constitutive equation for large strain elastoplasticity, Int. J. Eng. Sci. 20 (1982) 19–26.
[47] J.C. Simo, T.J.R. Hughes, Computational Inelasticity, Springer-Verlag, New York, Inc., 1998.
[48] K. Saanouni, Damage Mechanics in Metal Forming: Advanced Modeling and Numerical Simulation, John Wiley & Sons, 2012.
[49] F. Sidoroff, A. Dogui, Some issues about anisotropic elastic–plastic models at finite strain, Int. J. Solids Struct. 38 (2001) 9569–9578.
[50] P. Germain, Q.S. Nguyen, P. Suquet, Continuum thermodynamics, J. Appl. Mech. 50 (1983) 1010–1020.
[51] J. Lemaitre, J.-L. Chaboche, A. Benallal, R. Desmorat, Mécanique des matériaux solides, 3e édition, Dunod, Paris, 2009.
[52] J. Chaboche, A review of some plasticity and viscoplasticity constitutive theories, Int. J. Plast. 24 (2008) 1642–1693.
[53] K. Saanouni, J.-L. Chaboche, 3.06 – Computational damage mechanics: application to metal forming simulation, in: I.M.O.R. Karihaloo (Ed.), Comprehensive Structural Integrity, Pergamon, Oxford, 2003, pp. 321–376.
[54] D. Banabic, Sheet Metal Forming Processes: Constitutive Modelling and Numerical Simulation, Springer Science & Business Media, 2010.
[55] D. Banabic, H. Aretz, D. Comsa, L. Paraianu, An improved analytical description of orthotropy in metallic sheets, Int. J. Plast. 21 (2005) 493–512.
[56] D. Banabic, T. Kuwabara, T. Balan, D. Comsa, D. Julean, Non-quadratic yield criterion for orthotropic sheet metals under plane-stress conditions, Int. J. Mech. Sci. 45 (2003) 797–811.
[57] F. Barlat, J.C. Brem, J.W. Yoon, K. Chung, R.E. Dick, D.J. Lege, F. Pourboghrat, S.-H. Choi, E. Chu, Plane stress yield function for aluminum alloy sheets – part I: theory, Int. J. Plast. 19 (2003) 1297–1319.
[58] O. Cazacu, F. Barlat, Generalization of Drucker's yield criterion to orthotropy, Math. Mech. Solids 6 (2001) 613–630.
[59] O. Cazacu, F. Barlat, A criterion for description of anisotropy and yield differential effects in pressure insensitive metals, Int. J. Plast. 20 (2004) 2027–2045.
[60] J.W. Yoon, F. Barlat, R.E. Dick, K. Chung, T.J. Kang, Plane stress yield function for aluminum alloy sheets – part II: FE formulation and its implementation, Int. J. Plast. 20 (2004) 495–522.
[61] V. Cvitanic, F. Vlak, Z. Lozina, A finite element formulation based on non-associated plasticity for sheet metal forming, Int. J. Plast. 24 (2008) 646–687.
[62] M. Kuroda, V. Tvergaard, A phenomenological plasticity model with non-normality effects representing observations in crystal plasticity, J. Mech. Phys. Solids 49 (2001) 1239–1263.
[63] K. Runesson, Z. Mroz, A note on nonassociated plastic flow rules, Int. J. Plast. 5 (1989) 639–658.
[64] T.B. Stoughton, J.W. Yoon, On the existence of indeterminate solutions to the equations of motion under non-associated flow, Int. J. Plast. 24 (2008) 583–613.
[65] T.B. Stoughton, J.W. Yoon, Anisotropic hardening and non-associated flow in proportional loading of sheet metals, Int. J. Plast. 25 (2009) 1777–1817.
[66] A. Taherizadeh, D.E. Green, A. Ghaei, J.-W. Yoon, A non-associated constitutive model with mixed iso-kinematic hardening for finite element simulation of sheet metal forming, Int. J. Plast. 26 (2010) 288–309.